HHS Public Access

Author manuscript

Immunity. Author manuscript; available in PMC 2026 June 08.

Published in final edited form as:

Immunity. 2026 May 12; 59(5): 1454–1472.e9. doi:10.1016/j.immuni.2026.01.029.

Multiomic analysis of ART-interruption cohorts identifies cell-extrinsic and -intrinsic mechanisms driving lymphocyte-mediated control of HIV rebound

Tongcui Ma[1,2,17], **Ashley F. George**[1,2,17], **Zichong Li**[1], **Reuben Thomas**[1], **Kailin Yin**[1,2], **Min-Gyoung Shin**[1], **Mauricio Montano**[1], **Yusuke Matsui**[1], **Manickam Ashokkumar**[3], **Kyrlia Young**[1,2], **Julia Prigann**[1], **Julie Frouard**[1,2], **Sabrina Leddy**[4], **Maisha Adiba**[5], **Christina Herrde**[5], **Ulrike C. Lange**[5,6], **Cedric Feschotte**[4], **Douglas F. Nixon**[7], **Edward P. Browne**[3], **Nancie M. Archin**[3], **Jonathan Z. Li**[8], **Davey Smith**[9], **Steven Deeks**[2], **Ole S. Søgaard**[10], **Martin Tolstrup**[10], **Sulggi Lee**[2], **Satish K. Pillai**[2,11], **Mohamed Abdel-Mohsen**[12,13,14], **Katherine S. Pollard**[1,2,15], **Robert Siliciano**[16], **Melanie Ott**[1,2,15,*], **Warner C. Greene**[1,2,*], **Nadia R. Roan**[1,2,18,*]

[1]Gladstone Institutes, San Francisco, CA 94158, USA

[2]University of California, San Francisco, San Francisco, CA 94158, USA

[3]Department of Medicine, University of North Carolina at Chapel Hill, Chapel Hill, NC 27599, USA

[4]Department of Molecular Biology and Genetics, Cornell University, Ithaca, NY, USA

[5]Leibniz Institute of Virology, Hamburg, Germany

[6]Institute of Infection Research and Vaccine Development, University Medical Center Hamburg-Eppendorf, Hamburg, Germany

[7]Institute of Translational Research, Feinstein Institutes for Medical Research, Manhasset, NY 11030, USA

[8]Department of Medicine, Brigham and Women's Hospital, Boston, MA 02115, USA

[9]School of Medicine, University of California, San Diego, La Jolla, CA 92093, USA

[10]Department of Clinical Medicine, Aarhus University, Aarhus, Denmark

[11]Vitalant Research Institute, San Francisco, CA 94105, USA

[12]Division of Infectious Diseases, Department of Medicine, Feinberg School of Medicine, Northwestern University, Chicago, IL 60611, USA

[*]Correspondence: nadia.roan@gladstone.ucsf.edu (N.R.R.), melanie.ott@gladstone.ucsf.edu (M.O.), warner.greene@gladstone.ucsf.edu (W.C.G.).

AUTHOR CONTRIBUTIONS

Conceptualization/methodology, T.M., A.F.G., and N.R.R.; investigation, T.M., A.F.G., Z.L., K. Yin, M.M., Y.M., M.A., K. Young, J.P., S.K.P., and M.A.-M; software/formal analysis/visualization, T.M., R.T., M.-G.S., A.F., J.F., S. Leddy, M.A.-M., and E.P.B.; resources, J.Z.L., D.S., S.D., O.S.S., M.T., and S. Lee; supervision, U.C.L., C.F., D.F.N., E.P.B., N.M.A., K.S.P., R.S., M.O., W.C.G., and N.R.R.; funding, M.O., W.C.G., and N.R.R.; original draft writing, N.R.R.; writing/review/editing, T.M. All authors reviewed the final manuscript.

DECLARATION OF INTERESTS

The authors declare no completing interests.

[13]Center for Human Immunobiology, Department of Medicine, Feinberg School of Medicine, Northwestern University, Chicago, IL 60611, USA

[14]Potocsnak Longevity Institute, Department of Medicine, Feinberg School of Medicine, Northwestern University, Chicago, IL 60611, USA

[15]Biohub, San Francisco, CA 94158, USA

[16]Division of Infectious Diseases, Johns Hopkins University School of Medicine, Baltimore, MD 21205, USA

[17]These authors contributed equally

[18]Lead contact

SUMMARY

Immunological mechanisms regulating HIV rebound after antiretroviral therapy (ART) interruption remain unclear. We examined relationships between host factors, HIV reservoir, and HIV time-to-rebound after analytical treatment interruption (ATI) by characterizing pre-ATI peripheral blood mononuclear cells (PBMCs) from 75 ART-suppressed people with HIV (PWH) using high-parameter methods. Across interventional (CLEAR, TEACH, and REDUC) and non-interventional (A5345) cohorts, delayed rebound was not associated with intact HIV. Cohort-specific immune effectors were associated with delayed rebound. RNA sequencing of $CD4^+$ T cells from A5345 revealed that the mTOR inhibitor DDIT4 and zinc finger protein ZNF254 were associated with delayed rebound. *In vitro* and *in vivo* studies demonstrated that DDIT4 and ZNF254 suppressed HIV expression. Metformin induced DDIT4 and suppressed HIV expression in primary cells and cells from ART-suppressed PWH, suggesting that this affordable diabetes drug could be repurposed to silence HIV. Our results support the pursuit of both immune- and HIV-silencing strategies to achieve ART-free HIV remission.

Graphical abstract

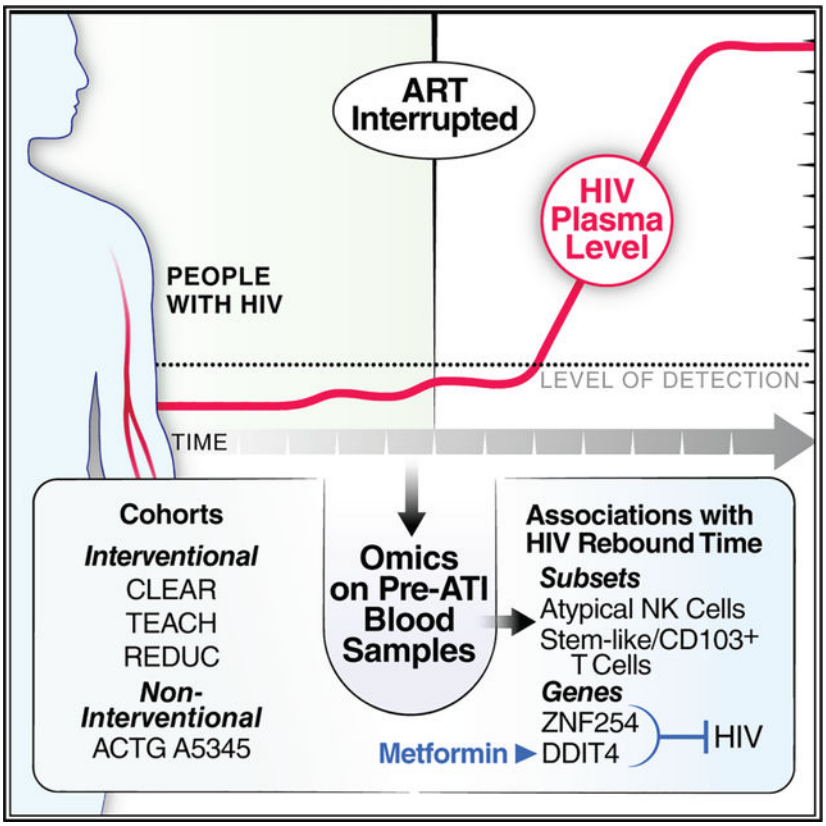

In brief

To identify factors that can mediate post-ART HIV control, Ma et al. performed “omics” on PBMCs from PWH from 4 analytical treatment interruption cohorts. NK and T cell features were identified, and the top two genes in $CD4^+$ T cells predicting delayed rebound were *ZNF254* and *DDIT4*—a metformin-inducible gene—which both silenced HIV expression *in vitro* and *in vivo*.

INTRODUCTION

Antiretroviral therapy (ART) has been transformative for people with HIV (PWH) but is not curative as it cannot eliminate the long-lived reservoir of HIV-infected cells. For most PWH, viremia typically rebounds within a period of a few weeks upon ART cessation.[1] There are, however, outliers who exhibit delayed rebound, including those termed post-treatment controllers (PTCs), who can maintain viral remission for months or even years after stopping ART.[2,3] Over the past decade, numerous analytical treatment interruption (ATI) trials have been performed, in the context of both trials that implemented therapeutic interventions[4–9] and those that did not.[10–17] Such studies have revealed that rebound time associates with features of both the reservoir and host immunity.

Recent efforts have assessed whether levels of genome-intact proviruses, particularly those measured with the intact proviral DNA assay (IPDA),[18] can predict timing of viral rebound. The rationale has been that intact proviruses are most likely to be replication-competent and hence capable of viral resurgence upon ART cessation. However, findings have

been inconsistent: while some found associations between intact proviruses and time-to-rebound,[19] others have not.[20,21] Finding such an association may also be context-dependent, as intact proviral DNA predicted fast rebound in those who initiated ART during the chronic but not acute phase of infection.[11] By contrast, high total proviral DNA is generally found to be associated with faster rebound.[12–15] Multiple studies have also found cell-associated HIV RNA to associate with faster rebound.[10,11,16,17,21,22] One study additionally found that in roughly half of participants who stopped ART, HIV polymerase (pol) sequences from rebound virus matched those found in cell-associated RNA prior to ATI.[23] These observations together suggest that the "active" reservoir (transcribing/translating HIV gene products) is a predictor of viral rebound time and includes rebound-competent virus, and is therefore an important target for HIV cure strategies.[24]

Compared with viral reservoir features, less is known about cellular features associated with HIV rebound time. Expression of exhaustion markers PD1, TIM3, and LAG3 on T cells[25] and frequencies of activated $CD8^+$ T cells[11] are associated with faster rebound in acute-treated individuals. Conversely, lower T cell activation and numbers of functional natural killer (NK) cells are associated with ART-free viral control.[20,25] However, the immunological mechanisms that can drive delayed viral rebound remain incompletely understood. Establishing this understanding can provide a roadmap to therapeutically elicit durable ART-free control of HIV and may help fine-tune biomarkers to effectively predict rebound time, which would have great utility for the field.

Our goal was to leverage a variety of "omics" tools to identify host immune responses that associate with viral rebound time upon ART cessation, and to relate these findings to HIV persistence measurements, using specimens from four recent ATI trials. Three were interventional trials performed in Denmark: CLEAR, wherein participants orally received the latency reversing agent (LRA) panobinostat[7]; TEACH, wherein participants received the TLR9 agonist lefitolimod as both an LRA and an immune-boosting agent[9]; and REDUC, wherein participants received therapeutic vaccination followed by intravenous administration of romidepsin as an LRA.[8] The fourth trial was the Advancing Clinical Therapeutics for HIV/AIDS (ACTG) trial A5345, wherein individuals underwent ATI in the absence of therapeutic intervention.[11] We set out to test two overall hypotheses: that unique phenotypic features of T and NK effector immune cells control the timing of viral rebound; and that delayed rebound reflects $CD4^+$ T cell-intrinsic mechanisms that promote silencing of HIV gene expression. We report evidence supporting both hypotheses, and in doing so identify two targetable suppressors of HIV gene expression whose manipulation may help achieve long-term, ART-free HIV remission.

RESULTS

Study design and IPDA measurements

Blood from a total of 34 participants from Danish cohorts CLEAR, TEACH, and REDUC, and 41 participants from non-interventional cohort ACTG A5345, were analyzed in the current study (Figure 1; Table S1, STAR Methods). Peripheral blood mononuclear cells (PBMCs) collected immediately prior to ATI were analyzed by RNA sequencing (RNA-seq) and cytometry by time-of-flight (CyTOF). For CyTOF, we focused on T and NK cells,

given their potential to recognize and eliminate HIV-infected cells (Tables S2–S4). As validation, we confirmed their differential expression patterns between cellular subsets using approaches previously described[26–29] (Data S1). Primary outcome was time-to-rebound post ATI, and secondary outcome was genome-intact proviral content as determined by IPDA.[18] IPDA data from ACTG A5345 were taken from a recently published dataset[11] (Figure S1A), and we performed IPDA from the three Danish cohorts. In all three, total HIV DNA content associated with faster time-to-rebound, but this only reached statistical significance for CLEAR (Figure S1B). Intact HIV DNA trended with faster rebound in CLEAR and TEACH and slower rebound in REDUC, but none of these associations were significant (Figure S1C). Defective HIV DNA, particularly hypermutated or 3′ defective, was associated with faster rebound in all three Danish cohorts (Figure S1D).

T cell predictors of time-to-rebound differ between CLEAR, TEACH, and REDUC

We first performed CyTOF on specimens from the three interventional cohorts. Focusing initially on T cells, we gated for the following classic T cell subsets: T central memory (Tcm), T transitional memory (Ttm), T effector memory (Tem), T resident memory (Trm), T regulatory (Treg), T follicular helper (Tfh), Temra, and T naive/T stem cell memory (Tn/Tscm), using strategies detailed in Data S1. Most subsets showed no association with time-to-rebound to ≥1,000 HIV RNA copies/mL, and those that did differed between cohorts. For instance, frequencies of $CD4^+$ Tfh and $CD4^+$ Temra predicted longer rebound time, and frequencies of $CD4^+$ Ttm and $CD8^+$ Tem shorter time, in REDUC only. In TEACH, frequencies of $CD8^+$ Tn/Tscm predicted longer time-to-rebound (Figures S2A and S2B). Moreover, different T cell subsets associated with intact proviral content in the different cohorts: frequencies of Tfh predicted lower proviral DNA in TEACH, while frequencies of $CD8^+$ Trm and $CD8^+$ Tn/Tscm predicted lower and higher proviral DNA, respectively, in REDUC (Figures S2C and S2D).

We next asked whether clustering would reveal more consistent correlations between T cell compartments and rebound time or intact proviral DNA. The Louvain method[30] identified 5 clusters (Figure 2A) which we named T-D1–T-D5 (“T” refers to T cell clusters, and “D” to Danish cohorts). Slower rebound was associated with cluster T-D2 frequencies in REDUC, but T-D4 frequencies in TEACH (Figure 2B). Associations with intact HIV were only observed in REDUC, where intact DNA frequencies were associated with lower frequencies of cluster T-D1 but higher frequencies of cluster T-D4 (Figure 2C).

We then examined phenotypic features of the two clusters predicting the favorable outcome of longer time-to-rebound (clusters T-D2 in REDUC and T-D4 in TEACH). Cluster T-D2 consisted of memory ($CD45RO^+CD45RA^-$) $CD4^+$ T cells highly expressing PD1 and CXCR5 (Figures 2D and 2E), suggesting they are primarily Tfh cells, consistent with our prior observation of Tfh frequencies associating with longer time-to-rebound in REDUC (Figure S2A). Cluster T-D2 also highly expressed activation markers OX40, CTLA4, and CD25, homing receptors CCR6 and CD29, and the alpha chain of the interleukin 7 (IL-7) receptor (CD127), which is associated with stemness and important for homeostatic proliferation (Figure 2E). Cluster T-D4 consisted of $CD8^+$ T cells that were $CD45RO^-CD45RA^+$ and highly expressed CCR7 and CD27 (Figures 2F and 2G),

suggesting their identity to be either Tn or Tscm.[31] In stark contrast to cluster T-D2, cluster T-D4 lowly expressed activation markers OX40, CTLA4, CD25, and HLADR, but exhibited elevated CD30, relative to total T cells (Figure 2G). In addition, homing receptor CXCR4 and stemness-associated marker BIRC5 were elevated (Figure 2G).

Overall, these results suggest inter-cohort heterogeneity in T cell features associated with rebound time.

In REDUC, CD56^{int}CD16^{+} NK cells are associated with accelerated time-to-rebound in opposition to CD56^{-}CD16^{+} cells

We then implemented an analogous approach to find associations with NK cells. Louvain clustering of NK cells, identified through a sequential gating strategy (Data S1), revealed 7 clusters we named NK-D1–NK-D7 (Figure 3A). We only observed significant associations with rebound time in REDUC, where cluster NK-D1 predicted faster, while cluster NK-D2 predicted slower, rebound (Figure S2E). However, neither of these clusters associated with intact HIV DNA (Figure S2F).

To gain further insight into the opposing effects of NK-D1 and NK-D2 in REDUC, we assessed their phenotypic features. Cluster NK-D1, which associated with the unfavorable outcome of faster rebound, predominantly included immature CD56^{int}CD16^{+} cells, the most abundant subset of NK cells in PBMCs (Figures 3B and 3C). In contrast to cluster NK-D1 as a whole, which was statistically associated with time-to-rebound, CD56^{int}CD16^{+} NK cells only trended with faster time-to-rebound in REDUC (Figure 3D). In contrast to cluster NK-D1, cluster NK-D2 was composed predominantly of CD56^{-}CD16^{+} cells, and the frequencies of both cluster NK-D2 and CD56^{-}CD16^{+} cells associated with slower rebound time (Figures 3E–3G). NK-D2 and NK-D1 cells displayed nearly opposite profiles of NK receptors: NK-D1 expressed elevated NKG2D, NKp46, NKp30, NKG2A, KIR3DL1, and 2B4 and lower KIR2DL1 and LILRB1, compared with total NK cells from REDUC (Figure 3H), whereas NK-D2 expressed lower NKG2D, NKp46, NKp30, NKG2A, and 2B4, and elevated KIR2DL1 and LILRB1 (Figure 3I). The contrasting patterns of NK receptor expression between clusters NK-D1 and NK-D2 may relate to their different differentiation states, as CD57, a marker of NK cell maturity,[32] was elevated in cluster NK-D1 but lowly expressed in cluster NK-D2 (Figure 3J).

The CD56^{-}CD16^{+} population is known to expand during HIV infection and although considered dysfunctional,[33] has also been demonstrated to promote development of broadly neutralizing antibody (bnAb) responses.[34] The mechanism driving the bnAb response appears to be indirect and mediated by the inability of CD56^{-}CD16^{+} cells to kill Tfh cells that promote development of bnAb responses, in contrast to canonical CD56^{+} NK cells, which can eliminate the Tfh cells.[34] We therefore assessed whether there were opposing relationships between the frequencies of clusters NK-D1 (mostly canonical CD56^{+} NK cells) or NK-D2 (mostly CD56^{-}CD16^{+} cells) and Tfh frequencies. Indeed, Tfh frequencies negatively associated with cluster NK-D1 frequencies but positively with cluster NK-D2 frequencies in REDUC (Figure 3K). Tfh frequencies also trended positively with anti-HIV antibody responses in REDUC (Figure 3L). These results support an overall model whereby delayed rebound in REDUC is mediated by increased frequencies of CD56^{-}CD16^{+} cells,

which unlike their CD56$^+$ counterparts are unable to hinder Tfh-mediated enhancement of robust antibody responses against HIV, or which alternatively may directly promote killing of infected cells given their ability to efficiently engage in antibody-dependent cellular cytotoxicity (ADCC).[35]

CD103$^+$ T cell frequencies predict increased time-to-initial-rebound viremia in ACTG A5345

We then performed a similar set of CyTOF analyses with ACTG A5345. Manual gating for classic T cell subsets did not reveal significant associations with time-to-rebound to ≥ 1,000 HIV RNA copies/mL (Figures S3A and S3B). As ACTG A5345 included an additional measurement of time to earliest detectable viremia (HIV RNA above limit of detection), we also assessed for subset association with this parameter and found positive associations with frequencies of CD4$^+$ Tcm, CD4$^+$ Trm, Tfh, and CD8$^+$ Trm (Figures S3C and S3D). No significant associations were found between T cell subset frequencies and intact HIV (Figures S3E and S3F), although CD4$^+$ and CD8$^+$ Trm as well as CD8$^+$ Ttm associated negatively with the percentages of intact provirus out of total HIV DNA (Figures S3G and S3H).

Louvain clustering identified 9 T cell clusters we named T-A1–T-A9 (“A” refers to ACTG A5345) (Figure 4A). Time-to-rebound to ≥ 1,000 HIV RNA copies/mL positively associated with size of cluster T-A5 (Figure S3I). By contrast, time-to-detectable HIV RNA associated positively with sizes of clusters T-A1 and T-A9 and negatively with size of cluster T-A4 (Figures 4B and S3J). Focusing initially on the cluster which had the most significant association (cluster T-A9), we noted that its size also associated negatively with intact HIV DNA, whether measured as numbers per million CD4$^+$ T cells or as percentage of total HIV DNA (Figures S3K, S3L, and 4C). By contrast, neither 3′ defective nor 5′ defective percentages exhibited such a negative association (Figure 4C). Cluster T-A9 was primarily memory cells (CD45RO$^+$CD45RA$^-$) (Figure 4D), and highly expressed Trm marker CD103, stemness marker CD127, and gut-homing receptor CCR6, but lowly expressed lymph node-homing receptor CCR7 (Figure 4E). As CD103 was only expressed in cluster T-A9 (Figure 4F), we assessed the extent to which T cells expressing it were sufficient to predict rebound time. Indeed, frequencies of CD103$^+$ T cells associated with time-to-detectable HIV RNA (Figure 4G). CD103$^+$ T cell frequencies also negatively associated with percentages of intact HIV but not defective HIV (Figure 4H). Although cluster T-A9 was uniformly CD103$^+$, cells in this cluster were a mix of CD4$^+$ and CD8$^+$ T cells. To assess whether the CD4$^+$ and CD8$^+$ subsets of cluster T-A9 exhibited similar associations, we separated cluster T-A9 into sub-cluster T-A9a (CD4$^+$) and sub-cluster T-A9b (CD8$^+$) (Figure S3M). Both sub-clusters associated with time-to-detectable HIV RNA (Figures S3N and S3O). Both sub-clusters also associated with percentages of intact HIV (Figures S3P and S3Q). The two sub-clusters exhibited phenotypic differences, in that T-A9a highly expressed co-stimulatory molecule CD28, while T-A9b highly expressed Trm markers CD49d and CD69 (Figure S3R and S3S), suggesting the CD8$^+$ T cell subset of cluster T-A9 to be more reminiscent of Trm cells than their CD4$^+$ T cell counterparts.

The data presented thus far suggest that the relative size of T-A9 was associated with favorable outcomes of delayed time until initial detectable viremia and lower intact HIV

reservoir. Given associations of inflammation with viral rebound kinetics,[1,21] we assessed whether the size of cluster T-A9 associated with inflammatory markers. Multiple markers of inflammation (sCD163, TNFa, MCP2, IL15, and IL23) associated negatively with the size of cluster T-A9 (Figure 4I), suggesting that having high numbers of cluster T-A9 cells associates with a lower state of inflammation. The size of cluster T-A9 also positively associated with higher frequencies of polyfunctional ($IFN\gamma^+TNF\alpha^+IL2^+CD107a^+$) Gag-specific $CD4^+$ T cell responses, but the opposite association was observed for polyfunctional Gag-specific $CD8^+$ T cell responses (Figure 4J). By contrast, no associations were observed with polyfunctional HIV pol- or envelope (env)-specific T cell responses (Figure 4K).

Besides cluster T-A9, other clusters associated with longer time-to-rebound were clusters T-A1 and T-A5 (Figures S3I and S3J). Cluster T-A1, associated with longer time-to-detectable HIV RNA, consisted of memory ($CD45RO^+CD45RA^-$) $CD4^+$ T cells (Figures S3T and S3U). These cells highly expressed stemness marker CD127, activation/co-stimulatory receptors CTLA4, CD28, and OX40, and homing receptors CD29 and CCR6 (Figure S3V). Cluster T-A5, associated with longer time-to-rebound to ≥ 1,000 copies/mL of HIV RNA, consisted of $CD8^+$ T cells that were $CD45RO^-CD45RA^+$ (Figures S3W and S3X). Of note, the phenotypic features of cluster T-A5 mirrored that of cluster T-D4 (Figure 2G), in that there was elevated expression of CCR7, CD27, BIRC5, CD30, and CXCR4, and low expression of OX40, CTLA4, and HLADR (Figure S3Y). To directly assess whether cluster T-A5 was the equivalent of cluster T-D4, we performed label transfer,[36] where clusters generated from different datasets can be linked to one another. This analysis confirmed cluster T-A5 is the equivalent of cluster T-D4 (Figure S3Z). Hence, a cluster of $CD8^+$ T cells characterized by elevated expression stemness-associated markers (CCR7, CD27, and BIRC5) and low expression of activation markers (OX40, CTLA4, and HLADR) with the exception of CD30, is associated with delayed rebound in both TEACH and ACTG A5345.

In contrast to the T cell dataset, Louvain clustering of the NK cells from ACTG A5345 did not identify associations between any NK clusters with either time-to-rebound or intact HIV DNA (Figure S4).

RNA-seq analysis of CLEAR, TEACH, REDUC, and ACTG A5345

As a parallel strategy, we implemented RNA-seq assessment of genes associated with time-to-rebound. Because the Danish cohorts revealed both T and NK cell features to associate with rebound time, we opted to perform RNA-seq on bulk specimens inclusive of both T and NK cells for these cohorts. Inter-cohort heterogeneity was observed in terms of genes associated with time-to-rebound (Figure S5A). In CLEAR, associations were mostly found with shorter time-to-rebound; genes showing these associations belonged to pathways related to mitochondrial and energy metabolism and to protein translation. In TEACH, pathways were mostly associated with longer rebound time; these included a variety of protein translation and metabolic pathways including cholesterol metabolism. In REDUC, pathways related to cell adhesion and immune signaling were associated with longer rebound times, while similar to CLEAR, mitochondrial and energy metabolism, as well as protein translation, were associated with shorter rebound times (Figure S5B).

Because CyTOF analysis of ACTG A5345 did not reveal any NK signatures associated with rebound time (Figure S4), we opted to focus RNA-seq analysis on not PBMCs but rather $CD4^+$ T cells because (1) multiple CD4-expressing clusters exhibited associations with rebound time (Figures 4 and S3), and (2) $CD4^+$ T cells are major reservoirs for HIV and hence their transcriptomic analysis could reveal insights into cell-intrinsic reservoir features that can suppress/delay rebound of HIV. The top gene predicting longer time-to-detectable HIV RNA was the gene for the long non-coding RNA *SNHG3*, while the top gene predicting longer time-to-rebound to ≥ 1,000 HIV RNA copies/mL was the protein-coding gene DNA damage-inducible transcript 4 (*DDIT4*), a negative regulator of mechanistic target of rapamycin (mTOR) signaling (Figure S5C). Pathway analysis revealed faster time-to-detectable HIV RNA to be associated with oxidative phosphorylation and mitochondrial activity, and faster time-to-rebound to ≥ 1,000 copies/mL of HIV RNA to be associated with lipid biosynthesis/metabolism and vesicle organization (Figure S5D). Given recent suggestions that the HIV reservoir may persist in granzyme B-expressing cytotoxic $CD4^+$ T cells,[37] we assessed for associations of *GZMB* and other cytotoxic effectors with time-to-rebound. Although none of these cytotoxic genes had any statistically significant associations, it was noteworthy that all of them trended with faster rebound time (Figure S5E), consistent with the notion of cytotoxic reservoir cells contributing to viral rebound upon ART cessation.

DDIT4 predicts longer rebound time in ACTG A5345 and suppresses HIV gene expression *in vitro* and *in vivo*

We first focused on *DDIT4*, the most statistically significant hit from our $CD4^+$ T cell analysis in ACTG A5345 (Figures 5A and 5B), given that DDIT4 is a negative regulator of mTOR signaling,[39] and mTOR signaling promotes HIV expression.[40–43] Mining public RNA-seq databases (STAR Methods), we found *DDIT4* is preferentially expressed in immune cells, particularly T cells, across a variety of tissues including spleen, lymph nodes, adipose tissue, and male and female reproductive tracts (Figure S6A). Among $CD4^+$ T cells, *DDIT4* expression is highest in omentum and lowest in gut (Figure S6B). Among peripheral blood $CD4^+$ T cells, *DDIT4* expression is highest in memory T cells including the Tfh, Th17, and Th2 subsets, and lowest in naive $CD4^+$ T cell subsets and Temra cells (Figure S6C).

Given the broad expression of *DDIT4* in $CD4^+$ T cells and its role of mTOR signaling, we hypothesized that the association of *DDIT4* expression with delayed rebound may be due to the ability of DDIT4 to restrict HIV expression. To test this hypothesis, we assessed whether DDIT4 can impact reactivation of HIV in the 5A8 Jurkat cell line model of HIV latency. Small interfering RNA (siRNA)-mediated knockdown of DDIT4 expression by ~50% did not reactivate HIV (Figure 5C). However, given the low baseline HIV gene expression in 5A8, we also assessed the extent to which DDIT4 knockdown could increase HIV gene expression following low-dose PMA (phorbol 12-myristate 13-acetate) treatment. Under these conditions, there was a significant increase in HIV gene expression upon DDIT4 knockdown (Figure 5C). To confirm the ability of DDIT4 to limit HIV reactivation in a more physiologically relevant model, we used a primary cell model of HIV latency (Figure 5D).[44] As with the 5A8 model, under conditions where ~50% DDIT4 knockdown was achieved,

basal HIV gene expression was not altered, while cells that were stimulated exhibited increased HIV gene expression upon DDIT4 knockdown (Figure 5E).

To further characterize the relationship between DDIT4 inhibition and mTOR signaling, we tested the effects of small molecule Torin1, an inhibitor of mTORC1 (one of the two complexes driving mTOR signaling), as well as the small molecule SMAP2, an activator of PP2A that ultimately drives inhibition of mTOR signaling (Figure 5F). We reasoned that if the increase in HIV gene expression induced by DDIT4 knockdown is mediated by activation of mTOR, then both Torin1 and SMAP2 should decrease the ability of the knockdown to increase HIV reactivation. Indeed, Torin1 had such an effect, and SMAP2 further increased Torin1's inhibition of HIV reactivation induced by DDIT4 knockdown (Figure 5G). Finally, to determine the extent to which DDIT4 can suppress HIV gene expression *in vivo*, we leveraged a recently published RNA-seq dataset generated from $CD4^+$ T cells from 191 ART-suppressed PWH.[38] We observed a significant negative association between *DDIT4* and HIV RNA, but not HIV DNA (Figure 5H).

Hence, DDIT4 expression is associated with suppression of HIV gene expression both *in vitro* and *in vivo*.

Metformin induces DDIT4 expression and suppresses HIV gene expression

Besides being a known inhibitor of mTOR, DDIT4 has also been reported to be induced by the type 2 diabetes drug metformin.[45] Given the interest in leveraging the anti-inflammatory effects of metformin to diminish chronic inflammation and promote healthy aging in PWH,[46,47] we next assessed whether metformin could increase DDIT4 expression and diminish HIV expression in $CD4^+$ T cells. Using a tissue-based primary cell model[48] (Figure 6A), we first assessed the effects of metformin on DDIT4 expression in T cells. We found that metformin increased DDIT4 expression in a dose-dependent manner, by up to >10-fold at the highest metformin dose tested (Figure 6B). Three days following infection, $CD4^+$ T cells (identified through a gating strategy to include those that have downregulated cell-surface CD4,[49] Figure 6C) that were treated with metformin exhibited a dose-dependent decrease in expression of the HIV LTR-driven reporter gene (Figures 6D and 6E). The diminished infection rates in the presence of metformin were not due to cytotoxicity, as metformin tended to increase viability (Figure 6F). At the highest concentration of metformin tested (10 mM), HIV infection rates were diminished by a mean of 37% ($n = 5$ donors) with no drop in viability (Figure 6G). Metformin also significantly diminished HIV reactivation in cells from ART-suppressed PWH, by a mean of 51% (Figures 6H and 6I). Given the relationship between metformin and mTOR signaling, we additionally examined whether the mTOR inhibitor Torin1 similarly diminished HIV reactivation in participant cells and found that this was indeed the case, although inhibition was less potent than that observed with metformin (Figure 6J).

ZNF254 predicts longer rebound time in ACTG A5345 and is a suppressor of HIV gene expression *in vitro* and *in vivo*

After *DDIT4*, the next statistically significant gene predicting increased time-to-rebound to ≥ 1,000 HIV RNA copies/mL in ACTG A5345 was *ZNF254* (Figures 7A and 7B). Like

DDIT4, *ZNF254* is expressed in T cells, although less preferentially so than *DDIT4* (Figure S6D). Among $CD4^+$ T cells, *ZNF254* expression is highest in stomach, and in stark contrast to *DDIT4* is undetectable in omentum (Figure S6E). Also in contrast to *DDIT4*, *ZNF254* is preferentially expressed among naive $CD4^+$ T cells relative to memory subsets (Figure S6F).

ZNF254 is a member of a large family of DNA-binding proteins called Kruppel-associated box (KRAB) zinc finger (ZNF) proteins. Like other members of this family, ZNF254 includes two conserved motifs: an N-terminal KRAB domain that recruits TRIM28 to modulate chromatin architecture and gene expression, and a C-terminal ZNF region that binds to specific DNA sequences (Figure 7C). Although ZNF254 has not previously been implicated in HIV persistence, other KRAB ZNFs—in particular ZNF10, ZNF304, ZNF350, ZNF417, and ZNF587—have been reported to silence HIV expression *in vitro*.[51–54] And although these five genes are expressed comparably to *ZNF254* in $CD4^+$ T cells across a variety of tissues (Figure S6G), expression did not significantly associate with time-to-rebound (Figure 7D). To determine whether ZNF254 can inhibit HIV expression, we knocked it down in cell line- and primary cell-based latency models. As for DDIT4, knockdown of ZNF254 increased reactivation of stimulated reservoir cells in both models (Figures 7E and 7F). Conversely, overexpression of ZNF254 decreased both baseline and tumor necrosis factor alpha (TNFα)-induced HIV transcriptional activity (Figures 7G and 7H). Lentiviral-mediated overexpression of ZNF254 in primary $CD4^+$ T cells similarly diminished HIV expression (Figure 7I).

We then assessed the extent to which the *in vivo* expression patterns of ZNF254 associate with HIV RNA expression. Like *DDIT4* (Figure 5H), *ZNF254* expression associated with diminished HIV RNA expression in the aforementioned RNA-seq dataset[38] but did not reach statistical significance (not shown). However, when we leveraged a single-cell RNA-seq (scRNA-seq) dataset of transcriptionally-active (HIV RNA^+) cells from three ART-suppressed PWH,[50] we found that for all three donors, HIV RNA^+ cells expressed significantly lower *ZNF254* than their HIV RNA^- $CD4^+$ T cell counterparts (Figure 7J). These data support a model whereby low expression of *ZNF254* enables active HIV gene expression from reservoir cells during ART.

Given these results, we hypothesized that individuals that naturally control HIV may do so in part through increasing ZNF254 expression to suppress HIV expression. Indeed, leveraging public RNA-seq datasets generated from $CD4^+$ T cells from elite controllers (ECs) vs. non-controllers,[55] we discovered that ECs preferentially expressed *ZNF254* (Figure 7K). These findings support the notion that $CD4^+$ T cell expression of ZNF254 can mediate ART-free control of HIV.

DISCUSSION

In this study, we leveraged pre-ATI specimens from four clinical trials in PWH to identify predictors of time-to-rebound upon ART interruption. Consistent with some[20,21] but not other[19] studies, we found intact HIV DNA did not predict time-to-rebound. In fact, in all the interventional cohorts we analyzed, defective proviral content were better predictors. These

observations prompted us to focus on the relationship between host responses and timing of viral rebound.

Most of the host associations we observed were cohort-specific, which was expected given the differences between the interventions (or lack thereof) the participants had undergone. CyTOF analyses revealed REDUC to harbor the most T and NK cell associations with time-to-rebound. This may be because this trial was the only one where participants had received a therapeutic vaccination with an LRA, which should impact the activity of both types of effector cells. Indeed, a subset of REDUC participants exhibited a boost in HIV-specific T cell responses following the intervention.[56] Three clusters associated with time-to-rebound to ≥ 1,000 HIV RNA copies/mL in REDUC: T-D2 ($CD4^+$ Tfh cells) and NK-D2 ($CD56^-CD16^+$ cells) with longer rebound time, and NK-D1 (mostly canonical $CD56^{int}CD16^+$ NK cells) with shorter rebound time. We postulate that these associations are all inter-related, and that the driver behind the control of rebound is the decreased ratio of the NK-D1 to NK-D2 cells. Cluster NK-D1 corresponds to the most abundant NK cells in blood, and although they can exert anti-HIV activity, they can also hinder the development of HIV bnAbs due to their ability to kill Tfh cells which are needed for bnAb maturation.[34] By contrast, atypical $CD56^-CD16^+$ cells (cluster NK-D2), which are enriched in PWH and often thought of as dysfunctional, have diminished cytolytic activity against Tfh cells.[34] We propose a model whereby the therapeutic vaccination elicited Tfh-helped antibodies, which benefited the participants with a higher ratio of the dysfunctional $CD56^-CD16^+$ to functional $CD56^{int}CD16^+$ NK cells, as these individuals could better mount a Tfh-mediated anti-HIV antibody response. Supporting this model are our observations that in REDUC, (1) Tfh frequencies associate with longer time-to-rebound; (2) Tfh frequencies negatively associate with frequencies of the functional $CD56^{int}CD16^+$ NK cells, and positively associate with the frequencies of the dysfunctional $CD56^-CD16^+$ cells; and (3) Tfh frequencies trend with anti-HIV antibody titers. The higher titers of anti-HIV antibodies may facilitate ADCC, perhaps even mediated by the $CD56^-CD16^+$ cells themselves, since despite being considered dysfunctional, these cells may have enhanced ADCC activity.[35] Our observation that this subset preferentially expresses LILRB1, an NK receptor that promotes killing of HIV-infected cells,[57] is also consistent with the subset having potential cytotoxic activity against HIV. Future studies testing how NK cells and antibody-mediated effector functions may work together to promote ART-free HIV control are warranted.

Notably, among T cell clusters, T-D4 was the most abundant in the individual with longest time-to-rebound (more than 22 weeks after ATI) in TEACH. Cluster T-D4 are $CD8^+$ T cells that are $CD45RO^-CD45RA^+CCR7^+CD27^+$, suggesting them to be either Tn or Tscm cells. Cluster T-D4 lowly expressed multiple activation markers (OX40, CTLA4, CD25, and HLADR), with the exception of CD30, which was elevated. Because CD30 is not expressed on Tn cells, we postulate cluster T-D4 to be composed primarily of Tscm cells, which can be induced to express CD30. The high expression of stemness-associated factor BIRC5 is also consistent with the Tscm identity.[58] Notably, the TEACH outlier participant with the prolonged time-to-rebound who had the highest relative numbers of cluster T-D4 cells has evidence of immune-mediated control—this individual had exceptional numbers of polyfunctional Gag-specific $CD8^+$T cells, and had 3 transient blips during ATI suggesting

the ability of the immune system to control rebound viremia.[9] Notably, cluster T-D4 exhibited almost the identical phenotype as ACTG A5345's cluster T-A5, which similarly associated with increased time-to-rebound to ≥ 1,000 HIV RNA copies/mL. And as in TEACH, ACTG A5345 included a controller (in this case who rebounded after more than 33 weeks post ATI), and who had the highest frequencies of this $CD8^+$ T cell subset. Based on these observations, we speculate that both clusters T-D4 and T-A5 include HIV-specific Tscm that can expand robustly post ATI and mediate a prolonged period of ART-free control. Alternatively, it is possible that these cells mediate antigen-independent suppression of HIV gene expression, a notable property of $CD8^+$ cells.[59] Future studies examining the anti-viral activity of CD30-expressing Tscm are warranted.

In ACTG A5345, the additional inclusion of time-to-first-detectable HIV RNA enabled us to compare the host factors predicting different rebound endpoints, and the associations were completely different: while cluster T-A5 associated with longer time-to-rebound to ≥ 1,000 HIV RNA copies/mL as discussed above, it did not associate with longer time-to-detectable HIV RNA, which instead associated with clusters T-A1 and T-A9. Cluster T-A9 exhibited the more significant association and could be defined by exclusive expression of CD103, an integrin component expressed on Trm cells that promotes their interaction and retention within epithelium.[60] Consistently, Trm cells, whether defined by just CD103 or the combination of CD69 and CD103, also associated with time-to-detectable HIV RNA. As the gene expression profile of $CD103^+$ T cells in blood is reminiscent of gut T cells,[61] it is possible that the CD103-expressing cluster T-A9 are T cells that are homing to or from the gut. We postulate that such gut-residing T cells could control viral reactivation in the gut, a major site of HIV persistence, and that the detectable HIV RNA measurement reflects tissue-based reactivation that occurs before the virus has a chance to replicate to higher titers in blood. High frequencies of the CD103-expressing T cells were also associated with lower systemic inflammation (sCD163, TNFa, MCP2, IL15, and IL23), which may be an indirect effect of being able to prevent viral rebound. Further supporting the notion of gut-targeting therapeutics as a strategy to achieve HIV remission are observations that vedolizumab intervention at the time of ART initiation to block gut-homing receptor $\alpha 4\beta 7$ resulted in a modest delay in time-to-HIV-rebound.[62]

Our study's RNA-seq analysis focused on genes predicting time-to-rebound to ≥ 1,000 copies/mL of HIV RNA, as it was the endpoint shared between all four trials, and also because it was the primary outcome previously analyzed.[7–9,11] The three Danish trial specimens were analyzed first, and given that bulk RNA-seq analysis of total PBMCs from these trials did not yield clear targets that could be tested in validation studies, we opted, for the ACTG A5345 specimens, to perform bulk RNA-seq on purified $CD4^+$ T cells. We reasoned that focusing on $CD4^+$ T cells may reveal reservoir-intrinsic features associated with delayed time-to-rebound. Indeed, the top two hits from this analysis were genes that appear to be potential mediators of viral suppression, albeit through different mechanisms.

The first of these hits, DDIT4, was validated as a suppressor of HIV expression by demonstrating that (1) its knockdown in both cell line and primary cell models of HIV latency promoted reactivation of HIV, through a mechanism involving mTOR; (2) endogenous HIV RNA but not DNA from $CD4^+$ T cells of ART-suppressed PWH

significantly associated with DDIT4 expression; (3) metformin increased DDIT4 expression in tissue T cells and reduced HIV infection rates without causing cellular toxicity; and (4) metformin diminished HIV reactivation in cells from ART-suppressed PWH. Our finding that metformin decreases HIV infection rates in tissue-derived $CD4^+$ T cells is consistent with studies in a Jurkat cell line, PBMCs, and humanized mice.[63] Paradoxically, however, a recent study suggested that metformin may increase p24 protein within infected PBMCs.[64] The reason for this apparent discrepancy is unclear, but may relate to experimental protocol differences (*ex vivo* stimulated PBMCs in[64] vs. unstimulated tonsils here) and/or to the ability of metformin to induce expression of tetherin,[64] which could trap any packaged virions onto the surface of cells resulting in an accumulation of p24 signal. Regardless, the link between metformin, DDIT4 expression, and time-to-rebound calls for further interrogation into the use of this common drug in the context of HIV cure strategies. Metformin has already been tested in PWH for its anti-inflammatory effects and its ability to decrease T cell exhaustion and delay epigenetic aging.[46,47,65] Furthermore, the LILAC cure study demonstrated that a 12-week course of metformin could decrease the HIV RNA/DNA ratio in $CD4^+$ T cells from colons of 8/13 ART-suppressed participants,[66] which would be consistent with metformin-mediated induction of DDIT4 to block HIV gene expression. That direct inhibition of mTOR in ART-suppressed PWH can diminish unspliced HIV RNA, albeit not reaching statistical significance,[41] along with our finding that Torin1 inhibits HIV reactivation in cells from ART-suppressed PWH, are also consistent with our model of DDIT4-mediated ART-free viral suppression through inhibition of mTOR. Of note, the association of *DDIT4* expression with rebound time to ≥ 1,000 copies/ml HIV RNA copies/mL, but not with time-to-first-detectable HIV RNA, suggests that DDIT4 may play a more important role in preventing systemic spread of HIV viremia than in preventing initial viral recrudescence, which likely originates within tissues as discussed above.

The second hit from our RNA-seq analysis of $CD4^+$ T cells was ZNF254. As for DDIT4, we had multiple lines of evidence supporting ZNF254's role in viral suppression beyond the association with time-to-rebound. First, knockdown of ZNF254 in cell line and primary cell models of HIV latency increased HIV reactivation. Second and conversely, overexpression of ZNF254 blocked HIV gene expression. Third, analysis of a recently generated scRNA-seq dataset of HIV RNA^+ cells from ART-suppressed PWH[50] demonstrated that *ZNF254* expression was significantly lower in the HIV RNA^+ $CD4^+$ T cells than their HIV RNA^- counterparts, which is consistent with the ability of ZNF254 to prevent HIV RNA expression among latently-infected reservoir cells. Finally, further *in vivo* support of the relevance of ZNF254 was our finding from RNA-seq datasets[55] that $CD4^+$ T cells from ECs express more ZNF254 than do their counterparts from non-controller PWH on ART; this could reflect preferential elicitation of ART-free viral suppression in ECs. Notably, other ZNF family members (ZNF10, ZNF304, ZNF350, ZNF417, and ZNF578) that have previously been reported to suppress HIV gene expression *in vitro*[51–54,65] did not associate with time-to-rebound in our dataset. The reason underlying the select association of ZNF254 is unclear and does not appear to stem from preferential expression of ZNF254 among $CD4^+$ T cells from blood and tissues. Of note, *ZNF* genes also serve as sites of HIV integration, and such integration sites are especially common among genome-intact HIV provirus (~23% in Lian et al.[67]). It is postulated that genome-intact HIV provirus at these sites is selected for over

time due to minimal expression of HIV gene products in the *ZNF* loci, which are generally heterochromatized. Indeed, *ZNF254* was reported to be in a region of lamina-associated domains (LADs), which contain mostly transcriptionally silent heterochromatin, and to harbor genome-intact HIV provirus.[67] Future studies should interrogate whether ZNF254 may be a more potent blocker of HIV gene expression than other ZNFs, and the impact of HIV integration into the *ZNF254* gene on ZNF254 expression.

In summary, our results support the notion that viral rebound following ART interruption can be influenced by the relative numbers of canonical $CD56^{int}CD16^{+}$ cells vs. CD562210032 NK cells, multiple subsets of T cells distinguished by expression of CD30 or CD103, and cell-intrinsic viral suppression mechanisms in infected $CD4^{+}$ T cells. The notion that pathways associated with viral suppression can lead to prolonged ART-free control is consistent with the notion that HIV RNA associates with time-to-rebound during ATI.[10,11,16,17,21,22] Since most HIV RNA derives from defective proviral genomes and hence would not be capable of driving rebound viremia,[68] increased HIV RNA may reflect a more dysfunctional immune system, and indeed HIV RNA associates with chronic inflammation and immune exhaustion in ART-treated PWH.[69–71] Future studies should examine the extent to which DDIT4 and ZNF254 can mediate post-ATI control in other cohorts, and test the therapeutic potential of targeting the pathways associated with these genes. For example, we propose the implementation of a placebo-controlled ATI trial testing the effects of metformin treatment both during ART and post ATI. We expect that beyond its potential to mediate viral suppression through DDIT4 induction, metformin may have additional benefits including increasing HIV-specific T cell effector function,[46,65] helping mediate antibody-mediated recognition of HIV-infected cells and ADCC,[64] and blocking homeostatic expansion of HIV reservoir cells by inhibiting mTOR.[41]

Limitations of the study

Our study has limitations. IPDA data can be noisy, and the assay can misclassify some proviruses as intact[72]; future studies should assess associations with intact proviral content measured using full-length proviral sequencing. Because bulk instead of scRNA-seq was used, we were not able to determine the extent to which the RNA-seq profiles predicting time-to-rebound were shared between the interventional and non-interventional cohorts. Finally, our overall cohort is small (75 individuals total) which resulted in some sub-group analyses having low "n" and some associations being driven by outlier datapoints, but small sample sizes are a general limitation of ATI studies, which are challenging and logistically impossible on a large scale.

RESOURCE AVAILABILITY

Lead contact

Further information and requests for resources and reagents should be directed to and will be fulfilled by the lead contact, Nadia Roan (nadia.roan@gladstone.ucsf.edu).

Materials availability

This study did not generate new unique reagents.

Data and code availability

The raw datasets generated for this study can be found in the public repository Dryad, and accessible via following link: https://10.5061/dryad.5qfttdzhh. This paper does not report original code. Any additional information required to reanalyze the data reported in this paper is available from the lead contact upon request.

STAR★METHODS

EXPERIMENTAL MODEL AND STUDY PARTICIPANT DETAILS

CLEAR participants had received 12 oral doses of 20 mg Panobinostat 3x/week every other week for 8 weeks, and exhibited a median time-to-rebound of 17 days (range 14–56).[7] TEACH participants had received subcutaneous injections of 8 doses of 60 mg of the TLR9 agonist MGN1703 2x/week for 4 weeks, and exhibited a median time-to-rebound of 17 days (range 14–151).[9] REDUC participants had received 6 doses of therapeutic peptide vaccine (BioNor) followed by 3 doses Romidepsin (1x/week for 3 weeks), and exhibited a median time-to-rebound of 21 days (range 10–56).[8] In all three interventional trials, the intervention induced transient changes in peripheral immune subset distribution or phenotypes.[56,73–75] CLEAR, TEACH, and REDUC participants all initiated ART during the chronic phase of HIV infection. ACTG A5345 participants consisted of those that initiated ART during chronic (n = 30) and acute (n = 11) infection who underwent ATI in the absence of any therapeutic interventions, and exhibited a median time-to-rebound of 22 days (range 13–230), and were a subset of those previously analyzed with sufficient banked specimen availability.[11] This study was approved by the institutional review boards of the corresponding institutes. The approval numbers for CLEAR, REDUC, and TEACH were 1-10-72-98-12, M-2013-364-13, and 1-10-72-10-15, respectively. The ACTG A5345 study was approved by the institutional review boards of each ACTG A5345 site. *Ex vivo* reservoir reactivation experiments entailed use of cryopreserved PBMCs from PWH obtained under UNC IRB # 08-1575.

METHOD DETAILS

HIV reservoir and RNA quantification: Total, intact, 3′ defective, and 5′ defective proviral HIV DNA was quantified in $CD4^+$ T cells from CLEAR, TEACH, and REDUC participants using the IPDA performed at AccelevirDx using methods previously described.[18] For ACTG A5345, recently reported IPDA measurements[11] were used in the current study. The primary outcome of time-to-rebound to ≥ 1,000 HIV RNA copies/ml were obtained from the original published CLEAR, TEACH, REDUC, and ACTG A5345 studies.[7–9,11] For ACTG A5345 we additionally included the parameter of weeks to detectable HIV RNA. This parameter corresponded to the number of weeks until ≥ 20 HIV RNA copies/ml or until <20 HIV RNA copies/ml but with target detected (above the limit of detection but below the lower limit of quantification), among the subset of ACTG A5345 participants who had no target detected prior to ATI.

Cell preparation for CyTOF staining: For each specimen, a total of 1–6 million cells were washed with PBS/EDTA (contaminant-free PBS from Rockland, supplemented with 2 mM EDTA), followed by a 60-second incubation at room temperature with 25 μM cisplatin

in 4 ml PBS/EDTA for subsequent assessment of cellular viability. The reaction was then quenched with 6 ml CyFACS (metal contaminant-free PBS from Rockland supplemented with 0.1% bovine serum albumin and 0.1% sodium azide). The cells were then fixed with 2% PFA diluted in metal contaminant-free PBS (Rockland), washed three times with CyFACS, and frozen at −80°C until CyTOF staining.

CyTOF antibody conjugation with metals: Antibodies necessitating in-house conjugation were conjugated to their respective metal isotopes using X8 antibody labeling kits, following manufacturer's guidelines (Standard BioTools). Briefly, metal was mixed with the polymer, and the mixture was incubated for 1 h at room temperature. During this incubation time, the unconjugated antibody was transferred into 50 kDa Amicon Ultra 500 µl V-bottom filters (Fisher) and subjected to R buffer exchange, followed by 30-minute reduction at 37°C using a 1:125 dilution of tris (2-carboxyethyl) phosphine (TCEP) from Pierce. Following two washes with C-buffer (Standard BioTools), the metal-loaded polymer and antibodies were resuspended within a 3 kDa and 50 KDa Amicon Ultra 500 µl V-bottom filter (Fisher), respectively. Subsequently, the metal-loaded polymer was transferred to the antibody and coupled for 2 hours at 37°C. After three washes, conjugated antibodies were quantified for protein content (Nanodrop). The conjugates were then diluted 1:1 with a PBS-based Antibody Stabilizer (Boca Scientific) supplemented with 0.05% sodium azide, and stored at 4°C until use.

CyTOF cell barcoding and staining: Cell barcoding was performed using the Cell-ID 20-Plex Pd Barcoding Kit in accordance with manufacturer's guidelines (Standard BioTools). Briefly, for each sample, a total of 1–3 million cells was washed twice with Barcode Perm Buffer (Standard BioTools). The appropriate barcode was then added at a ratio of 1:90 and incubated with the cells for 30 minutes. Cells were then washed once with 0.8 ml Maxpar™ Cell Staining Buffer (Standard BioTools), followed by a second wash with CyFACS. The barcoded samples were next blocked for 15 minutes on ice using sera derived from mouse (1:33 dilution, Thermo Fisher), rat (1:33 dilution, Thermo Fisher), and human (1:166 dilution, AB serum, Sigma-Aldrich) in CyFACS. The cells were then washed twice with CyFACS buffer, and stained for 45 minutes on ice with CyTOF surface staining antibody cocktails (Tables S2–S4) in a total volume of 100 µl per well. Following a series of three sequential washes with CyFACS buffer, the cells were fixed overnight at 4°C with 2% paraformaldehyde (PFA, Electron Microscopy Sciences) diluted in metal contaminant-free PBS (Rockland). The next day, cells were permeabilized by a 30-minute incubation at 4°C using fix/perm buffer (eBioscience), followed by two washes with Permeabilization Buffer (eBioscience). Cells were then blocked for 15 minutes on ice with sera from mouse (1:6.7 dilution, Thermo Fisher,) and rat (1:6.7 dilution, Thermo Fisher) in CyFACS. After two washes with Permeabilization Buffer (eBioscience), the cells were stained for 45 minutes on ice with the CyTOF intracellular staining antibody cocktail (Tables S2–S4). Cells were then washed once with CyFACS, and incubated for 20 minutes at room temperature with 250 nM Cell-ID™ DNA Intercalator-Ir (Standard BioTools) in 2% PFA diluted in metal contaminant-free PBS (Rockland). The cells were then washed twice with CyFACS, followed by sequential washing with Maxpar® Cell Staining Buffer (Standard BioTools), Maxpar® PBS (Standard BioTools), and Maxpar® Cell Acquisition

Solution (Standard BioTools). Immediately before data acquisition, cells were resuspended at a concentration of 7×10^5/ml in EQ™ calibration beads (Standard BioTools) diluted in H_2O. Cell acquisition was performed at a rate of 250–350 events/sec on a CyTOF2 instrument (Standard BioTools) at the UCSF Parnassus FACS Core.

CyTOF data processing: Raw CyTOF datasets were normalized to EQ™ calibration beads, and de-barcoded using CyTOF software provided by Standard BioTools. The normalized data were then imported into both FlowJo (BD Biosciences) and Cytobank for gating and phenotyping analysis. Total T cells and NK cells were identified through sequential gating strategies following gating from live, intact singlet cells as depicted in Figures S1 and S2. Raw datasets corresponding to these gated events are available for download as FCS files from the following link in the Dryad public repository: https://datadryad.org/dataset/doi:10.5061/dryad.5qfttdzhh. For clustering, these gated events were exported as csv files for downstream analyses.

CyTOF data pre-processing and clustering: The arcsine-transformed data for a given CyTOF panel across all the cells derived from the samples in a given cohort were combined into a single Seurat R object.[36,76–79] A Principal Component Analysis (PCA) embedding for each of the resulting cells of dimension equal to the number of markers in the panel was generated using the *RunPCA* function in Seurat applied to the scaled arcsine-transformed data. A 2D UMAP-based[80] visualization of the data was then derived from this PCA embedding. Biological variables (e.g., viral rebound week, intact over total HIV RNA copies, sex, ethnicity) and technical variables (processing batch) were visualized in the resulting UMAPs. Besides the presence of batch effects in the NK cell data from the Danish cohort as determined by visual inspection of the corresponding UMAP, batch effects were not evident. Hence, a second batch-corrected cell embedding for the NK cells in the Danish cohort was determined after running the *RunHarmony* function that is part of the Harmony package.[81] The clustering of cells based on similar marker profiles in each data set was determined using the *FindClusters* function implementing the Louvain method[30] that was either applied to the Harmony-based embedding (for the NK cells in the Danish cohort) or the PCA embedding for all other datasets. The optimal clustering resolution parameters for this clustering in each dataset were determined using Random Forests[82] and a silhouette score-based assessment of clustering validity and subject-wise cross-validation, as previously implemented.[83,84] This Louvain-based method prevents over- and under-clustering by using a Leave-One-Out-Cross-Validation (LOOCV) method to predict cluster membership. The method fits cells from all but one of the subjects, and then evaluates the resulting predicted clusters of the cells from the held-out subject using the Average Silhouette Width (ASW) clustering metric. The resolution parameter in the Louvain algorithm is identified that maximizes both the mean (across all samples) of the Average (across cells within each sample) Silhouette Width (ASW) of the resulting clusters, along with the local maxima, while also taking into account prior biological domain knowledge when appropriate. Using this procedure, the optimal resolution parameters for both the NK cell and T cell panels in the Danish cohorts was determined to be 0.06, while for the ACTG A5345 cohort they were equal to 0.2 for the T cell panel and 0.13 for the NK cell panel. The markers for each cluster were determined using the *FindAllMarkers* function in Seurat. The

average expression for each marker was determined using the AverageExpression function in Seurat. Clusters that contained less than a total of 1,000 cells were excluded from further analyses. Heatmap depiction of expression of protein antigens within each cluster is presented in Figure S7.

CyTOF cluster association analysis: A generalized linear mixed model (GLMM) implemented in the lme4[85] package in R with the family argument set to the binomial probability distribution was used to estimate the association between cluster membership and each of the variables (viral rebound week, intact proviral frequencies, cytokine and plasma protein content, and HIV immune-specific responses). A sample-specific random effect was included to model the inter-sample variability in terms of change in log odds of cluster membership for samples with the same set of covariates. Subsets were either defined as manually gated groups of cells or via the Louvain clustering method. Sample-specific cluster memberships were defined as the proportion of cells derived from each of the samples in the cluster. The change in cluster membership per unit change in variable was estimated as a log odds ratio, defined as the change in the log odds of cluster membership per unit change in the variable. This was estimated with the emmeans R package[86] using the GLMM model fit. Separate associations for each of the samples in each of the three trials were estimated for the Danish cohorts. The models used for ACTG A5345 were adjusted for sex and ethnicity. The association of memberships of two cluster definitions for the samples in the same cohort was determined using spearman correlation of logit-transformed proportions.

Label transfer analysis: The T cell clusters defined for ACTG A5345 were linked to clusters defined in CLEAR, TEACH and REDUC using the label transfer approach[36] where anchor cells were first determined between the two datasets in 20-dimensional PCA space using scaled log-normalized data for the two cohorts by implementing the *FindTransferAnchors* function. Linked clusters were then identified using the *TransferData* function.

Plasma profiling: Anti-HIV antibody responses were measured using the Luciferase Immunoprecipitation Systems (LIPS) assay.[87] This assay measures binding of plasma antibodies to luciferase fusion proteins, and raw light units are log-transformed for better visualization. Our dataset had LIPS units within the range of 4.0–6.5, corresponding to raw light units of $10^{4.0}$–$10^{6.5}$. Targeted proteomic profiling was used to quantitate 247 soluble markers in plasma samples using the NULISAseq Inflammation Panel 250 (Alamar Biosciences) according to the manufacturer's protocols as previously described.[88]

HIV-specific T cell responses: A quantitation of HIV-specific T cell responses by FACS was recently published[11] and associated with the abundance of cluster T-A9 cells for the current study.

RNA-seq data generation: Cryopreserved PBMCs were rapidly thawed in a 37°C water bath, and then washed once with complete RPMI (Corning) containing 20% FBS (Avantor), 2 mM L-glutamine (Gibco), 100 μg/ml Penicillin-streptomycin (Gibco) and 10 mM HEPES (Gibco). The PBMCs were then resuspended in 10 ml of RPMI with 20%

FBS and transferred to 15 mL conical tubes. The cells were treated with 10 μL of RNase free DNase I (Sigma) (10 units/μl). After washing once with 10 ml of Ca^+/Mg^+-free PBS (Corning) containing 2% FBS, cells were stained with trypan blue solution and counted using a Bio-Rad TC-20 cell counter. Final PBMC cell numbers from each participant sample ranged from 7×10^6 to 25×10^6, with cell viability counts ranging from 70% to 96%. For specimens belonging to ACTG A5345, $CD4^+$ T cells were purified using the EasySep™ Human $CD4^+$ T Cell Isolation Kit from StemCell Technologies following the manufacturer's protocol. Total RNA was extracted from PBMCs (CLEAR, TEACH and REDUC) and $CD4^+$ T cells (ACTG A5345) using the Qiagen RNeasy Micro Kit per manufacturer's protocol. RNA yields ranged from 300 ng to 3,500 ng. RNA quality was tested using a Qubit 2 fluorometer (Thermo Scientific). Sequencing libraries were prepared by Azenta Life Sciences employing the NEB Next Ultra II RNA Library Prep Kit for Illumina. Briefly, mRNA was enriched using oligo (dT) beads, then fragmented for 15 minutes at 94°C followed by cDNA synthesis. Fragments were then end-repaired and adenylated. Universal adapters were ligated to cDNA fragments, then indexes were added with library enrichment by PCR. RNA integrity and library size was assessed by Agilent Tapestation, and concentrations were determined by Qubit 2 fluorometer with final quantification by qPCR. Flow cells were prepared with multiplexed and clustered sequencing libraries, then loaded onto an Illumina HiSeq instrument. Illumina HiSeq sequencing used a 2 × 150 bp, single index configuration with an estimated data output of ~350 M raw paired-end reads per lane. HiSeq Control software was used for base calling and image analysis. Raw data were delivered in FASTQ format, and are deposited in the Gene Expression Omnibus (GEO) database under accession number GSE290636.

RNA-seq and IPDA association analyses: The preprocessing of the raw sequencing reads from the samples in the Danish cohorts was run on a custom bioinformatics pipeline while the preprocessing for the samples in the ACTG cohort was run on the nf-core/rnaseq[89] pipeline. Sequencing reads were trimmed for known adapters and low-quality regions of reads using Fastq-mcf[90] for the Danish samples and Trim-galore[91] for the ACTG A5345 samples. For both sets of samples, sequence quality control was assessed using FastQC[92] and RSeQC.[93] Alignment of reads of both sets of samples to the human hg38 genome was performed using STAR.[94] Reads for the Danish samples were assigned to genes using "featureCounts"[95], part of the Subread suite (http://subread.sourceforge.net/). Transcript content for the ACTG A5345 samples were quantified using Salmon[96] and summarized as gene counts using tximport.[97] The *filterByExpr* function in the edgeR bioconductor package[98] with the min.count argument set to 5 was used to filter out lowly expressed genes. Principal Component Analysis (PCA) plots using the $\log_2$-transformed Counts-Per-Million (CPM) of the top-500 most variable genes revealed an outlier sample among the ACTG A5345 samples, which was removed from further analysis. Gene-wise dispersion values were estimated using a quasi-likelihood (QL) method implemented in the *glmQLFit* function in edgeR. The association of gene expression with time-to-viral-rebound to ≥ 1,000 HIV RNA copies/ml and to the number of intact proviruses per million $CD4^+$ T cells was estimated using an empirical Bayes quasi-likelihood F-based test (*glmQLFTest*)[99] separately in each of the three Danish trials (TEACH, CLEAR and REDUC). No adjustments were made for sex and ethnicity because the samples were all European and mostly male

(only two of the 34 samples were female). For the ACTG A5345 samples, the association between gene expression and time to detectable HIV RNA and time-to-rebound to ≥ 1,000 HIV RNA copies/ml, number of intact proviruses per million $CD4^+$ T cells, and ratio of intact HIV DNA to total HIV DNA was estimated using the *glmQLFTest*[99] function after adjusting for sex and the clinic from which the sample was derived. The clinic variable was used as a potential confounder of the associations since there was better clustering of gene expression profiles of samples by their clinic variable than by ethnicity. Volcano plots showing the results of these association analyses were generated using the *EnhancedVolcano* bioconductor package.[100] Enrichment of Gene Ontology-based gene sets[101,102] and *WikiPathways* gene sets[103] was assessed using the GSEA function in the *clusterProfiler* package.[104] Genes were selected for pathway analysis based on a raw p-value threshold of 0.05 for differential expression values. Pathways were considered significantly enriched if their Benjamini-Hochberg–adjusted p-values were below 0.1.

Analysis of *DDIT4* and *ZNF254* expression across cellular subsets in tissues: Four public databases were used to assess expression of *DDIT4*, *ZNF254*, and other ZNF genes in cellular subsets across human tissues: the Human Protein Atlas (https://www.proteinatlas.org/), the Tabula Sapiens dataset (https://tabula-sapiens.sf.czbiohub.org/), and two RNAseq datasets of $CD4^+$ T cell subsets generated from PBMCs.[105,106] Single cell-type clusters were normalized separately from other transcriptomics datasets using Trimmed mean of M values (TMM) following the Human Protein Atlas normalization process. To generate expression values per cell type, clusters were aggregated per cell type by first calculating the weighted mean normalized transcript expression values (nTPM) in all cells with the same cluster annotation within a dataset. The values for the same cell types in different data sets were then mean-averaged to a single aggregated value. Only clusters with medium and high reliability were included. For the PBMC datasets, nTPM values below 0.1 were not visualized. For the Tabula Sapiens dataset, which were pre-normalized, the filters applied were: Disease type = Normal, and Cell type = CD4-positive helper T cells.

siRNA knockdown experiments: siRNAs for DDIT4 (L-010855-01-0005) and ZNF254 (L-019877-02-0005) were purchased from Horizon, while the negative control siNegative was purchased from ThermoFisher (4390843). For every million J-Lat 5A8 cells,[107] 30 pmol siRNA was introduced using SE Cell Line 4D- Nucleofector X Kit L (Lonza V4XC-1024) and the CL-120 program of the Lonza 4D-Nucleofector X Unit (AAF-1002X). The cells were treated with 5 nM PMA (Selleckchemor, S7791) or DMSO one day after nucleofection, and assessed one day later for GFP using a BD LSRFortessa™ X-20 flow cytometer. Latently-infected primary $CD4^+$ T cells were generated using a single-round HIV GFP reporter virus as previously described.[44] For every 10^7 primary cells, 30 pmol siRNA was introduced using P3 Primary Cell 4D-Nucleofector X Kit L (Lonza V4XP-3024) and the E0–115 program of the of the Lonza 4D-Nucleofector X Unit (AAF-1002X). One day after nucleofection, half of the cells were maintained in resting conditions, and the other half were activated with 1 μg/ml anti-CD28 antibody (BD Biosciences 555725) in 12-well plates coated with anti-CD3 antibody (BD Biosciences 555336). Where indicated, 10 nM Torin (Selleckchem S2827) and/or 5 μM SMAP-2 (MedChemExpress HY-120272)

(or DMSO as negative control) were added. One day later, GFP levels were assessed using BD LSRFortessa™ X-20 flow cytometer.

Western blot: A total of 0.2 million J-Lat cells 5A8 or 1 million primary cells were lysed in 20 μl Laemmli buffer and loaded per lane. Human lymphoid aggregate culture (HLAC) cells were positively selected for $CD3^+$ cells using the EasySep™ Human CD3 Positive Selection Kit II prior to western blotting. The primary antibodies used for western blotting were mouse anti-human α-tubulin (Sigma CP06), rabbit anti-human CDK9 (Bethyl A303–493A), rabbit anti-human DDIT4 (Bethyl A302–169A), and mouse anti-human ZNF254 (Novusbio H00009534-B01P). The secondary antibodies were goat anti-mouse-680 nm (Thermo Fisher A-21057) and goat anti-rabbit-680 nm (Thermo Fisher A-21076). Primary antibodies were diluted to 1 μg / ml with the exception of α-tubulin, which was used at a concentration of 200 ng / ml. All secondary antibodies were diluted 10,000-fold.

Tonsil infection assays: Tonsils from healthy donors were obtained from the Cooperative Human Tissue Network (CHTN) and processed into HLACs as previously described.[26,48] The cells were then incubated with media alone or the indicated concentrations of metformin (Sigma-Aldrich, PHR1084) for 24 hours. Some cells were set aside to establish the effects of metformin on cellular cytotoxicity using a lactate dehydrogenase (LDH) assay (Roche). The remaining cells were then mock-treated or exposed to 100 ng / ml of $p24^{Gag}$ of the F4.HSA reporter virus.[48] Three days later, cells were treated with Fc block (BioLegend, 422302), and stained with the panel of antibodies listed in Table S5. Following fixation with 2% PFA (Electron Microscopy Science, 15710), cells were analyzed on a BD LSRFortessa™ X-20 flow cytometer to monitor infection rates and final cellular viability.

***Ex vivo* reservoir reactivation assays using cells from PWH:** Cryopreserved PBMCs from PWH who had initiated ART during the chronic phase of infection and had been virally suppressed for at least 9 years (Table S6) were obtained. The cells were revived for 24 hours in RPMI media containing 1 μM Raltegravir and 4 μM Abacavir to prevent spreading infection. $CD4^+$ T cells were then isolated using the EasySep™ Human $CD4^+$ T Cell Isolation Kit (StemCell Technologies) and cultured in media supplemented with 5 U/mL IL2. $CD4^+$ T cells were then treated with media alone or 10 mM metformin (Sigma-Aldrich, PHR1084) or 10 nM Torin1 (Selleckchem S2827) for 24 hours, and then stimulated with 10 nM PMA (Sigma-Aldrich) and 500 nM ionomycin (Sigma-Aldrich). Cells were harvested at 24 hours post-stimulation for quantification of Gag expression by qRT-PCR as previously described.[108] Briefly, RNA was extracted from the treated cells using the RNeasy plus kit (Qiagen), and 1 μg of Nanodrop-quantified RNA from replicates of each condition were reverse transcribed and amplified using Fastvirus (Thermo, Waltham, MA) and primer sets for HIV Gag RNA (GAG-F: ATCAAGCAGCCATGCAAATGTT, GAG-R: CTGAAGGGTACTAGTAGTTCCTGCTATGTC, GAG Probe: FAM/ZEN-ACCATCAATGAGGAAGCTGCAGAATGGGA-IBFQ). The Quant Studio 3 Real-Time PCR system thermocycler (Applied Biosystems) was used for the quantification. Cycling parameters were 5 min reverse transcription step at 50°C, 95°C for 20 sec for Taq activation, followed by 40 cycles of 95°C (3 sec.), and 60°C (30 sec.). Normalized relative expression was

calculated using the Prism software version 10.1.1 (GraphPad). Experiments were performed as experimental triplicates for each donor.

ZNF254 overexpression studies: VSV-G-pseudotyped lentiviral vectors encoding either an empty vector or ZNF254–3xHA[109] under the control of a Tet-inducible promoter were co-transfected with psPAX2, pCMV-VSV-G, and the respective transfer vector using the CalPhos Mammalian Transfection kit (Takara) in 293T cells according to manufacturer's instruction. Lentiviral particles collected from the supernatants were then used to transduce J-Lat 11.1 cells[110] followed by selection with 1 μg/ml puromycin (Thermo Fisher). For reactivation experiments, ZNF254-expressing and control J-Lat 11.1 cells were cultured for 4 days in RPMI supplemented with 250 ng/ml Doxycycline (StemCell Technologies) before treatment with indicated concentrations of TNFα (Peprotech) for 16 hours. For overexpression in primary cells, lentiviral vectors encoding ZNF254 (ZNF254-V5-SBP-ΔLNGFR) or BFP are a negative control (BFP-V5-SBP-ΔLNGFR) were produced by combining psPAX2, pCMV-VSV-G,[111] and the corresponding transfer vector at a ratio of 3.25:1:3.25, and transfecting Lenti-X 293T cells (Takara Bio) for 24 hours with polyethylenimine (PEI, Polysciences) in Opti-MEM™ (Fisher Scientific) followed by replacement of culture medium supplemented with medium containing 1 mM sodium butyrate (Sigma-Aldrich), and harvesting of supernatants 3 days later. For generating HIV-infected primary cells, $CD4^+$ T cells were isolated from PBMCs of n=3 HIV-seronegative donors using the EasySep™ Human $CD4^+$ T Cell Isolation Kit (StemCell Technologies) and activated using the ImmunoCult™ Human CD3/CD28 T Cell Activator (StemCell Technologies) for 4 days. The cells were then infected with a VSV-G pseudotyped HIV GFP reporter virus (HIVd6EGFP), produced by co-transfecting Lenti-X 293T cells with psPAX2, pCMV-VSV-G, and pNL4–3-Δ6-drEGFP[111] using the TransIT-LT1 Transfection Reagent (Mirus Bio). Ten days later, cells were stimulated again with the ImmunoCult™ Human CD3/CD28 T Cell Activator, and then transduced with ZNF254-V5-SBP-ΔLNGFR or BFP-V5-SBP-ΔLNGFR. Transduced cells were cultured for 7 days prior to treatment for 16 hours with media alone, or with 50 ng/mL PMA (Sigma-Aldrich) and 1 μM ionomycin (Sigma-Aldrich). All J-Lat and primary cells were monitored for GFP expression using a BD LSRFortessa™ X-20 flow cytometer.

QUANTIFICATION AND STATISTICAL ANALYSIS

Associations between numeric meta-data variables were determined using Spearman correlation coefficients. We reported all significant associations that met a raw, unadjusted p-value threshold of 0.05, and further highlighted associations that met the False Discovery Rate (FDR)[112] multiple testing correction threshold of 0.05. Select associations were further validated using orthogonal assays. For associations of rebound time with IPDA measurements, undetectable IPDA values in ACTG A5345 were valued at zero. For defining genes differentially expressed in selected clusters, Wilcoxon Signed-Rank tests were used and adjusted for multiple comparisons using the FDR-based Benjamini-Hochberg method. The DFBETAS parameter[113] was used to estimate the influence of an extreme observation for given statistical associations. This parameter tests the scaled difference in the slopes of the respective linear associations that are estimated with the inclusion of the extreme observation. An observation was deemed influential for a given association when its

value was greater than 2/sqrt(N) where N is the number of observations used to estimate this association. Analysis of the DFBETAS parameter demonstrated that the associations reported in Figures 3D, 3E, 3G, and S2D were not driven by the outlier datapoints. In knockdown studies of DDIT4 and ZNF254, one-way ANOVA with Bonferroni correction for multiple comparisons were performed. Metformin studies were analyzed using one-way ANOVA followed by Tukey's multiple comparisons test or Mann-Whitney U test as indicated. Student's t-test were used for assessing *ex vivo* effects of drugs on cells from PWH. Student's t-test and Welch's t-test with Holm-Sidak correction were used to assessing on ZNF254 over-expression. Welch's *t*-tests were used to compare *ZNF254* expression in HIV^+ versus HIV^- $CD4^+$ T cells, and in $CD4^+$ T cell subsets from ECs vs. non-controllers. For all analyses, p-values less than 0.05 were considered statistically significant.

Supplementary Material

Refer to Web version on PubMed Central for supplementary material.

ACKNOWLEDGMENTS

We thank the A5345 study participants, the A5345 study team, as well as the site staff at the ACTG clinical research sites. We thank Jane Srivastava, Kevin Pastores, and Nandhini Raman (Gladstone Flow Core); Stanley Tamaki, Claudia Bispo, Vinh Nguyen, and Pricsilla Sanchez (Parnassus Flow Core); Françoise Chanut (editing); John Carroll (graphics); and Robin Givens (administrative) for their assistance. K.S.P. and M.O. are Biohub, San Francisco Investigators, and M.O. is the Nick and Sue Hellman Distinguished Professor. We gratefully acknowledge support from the Michael Hulton Center for HIV Cure Research. Financial support was also provided by The James B. Pendleton Charitable Trust and NIH grants R01-AI183286, R01-DK131526, R01-AI147777, R01-AG092241, R01-AI189353, R01-AI165079, R01-DK123733, P01-AI169606, P01-AI131374, P01-AI169768, R21-AI172060, UM1-AI164559, UM1-AI164567, UM1-AI068636, UM1-AI068634, UM1-AI106701, UM1-AI126620, S10-RR028962, P30-AI027763, P30-DK063720, and S10-OD018040, and The Gates Foundation grant NV-033977 and the HIV Reservoir Consortium (HIVRC).

REFERENCES

1. Giron LB, and Abdel-Mohsen M (2022). Viral and Host Biomarkers of HIV Remission Post Treatment Interruption. Curr. HIV/AIDS Rep 19, 217–233. 10.1007/s11904-022-00607-z. [PubMed: 35438384]
2. Namazi G, Fajnzylber JM, Aga E, Bosch RJ, Acosta EP, Sharaf R, Hartogensis W, Jacobson JM, Connick E, Volberding P, et al. (2018). The Control of HIV After Antiretroviral Medication Pause (CHAMP) Study: Posttreatment Controllers Identified From 14 Clinical Studies. J. Infect. Dis 218, 1954–1963. 10.1093/infdis/jiy479. [PubMed: 30085241]
3. Sáez-Cirión A, Bacchus C, Hocqueloux L, Avettand-Fenoel V, Girault I, Lecuroux C, Potard V, Versmisse P, Melard A, Prazuck T, et al. (2013). Post-treatment HIV-1 controllers with a long-term virological remission after the interruption of early initiated antiretroviral therapy ANRS VISCONTI Study. PLOS Pathog. 9, e1003211. 10.1371/journal.ppat.1003211. [PubMed: 23516360]
4. Archin NM, Kirchherr JL, Sung JA, Clutton G, Sholtis K, Xu Y, Allard B, Stuelke E, Kashuba AD, Kuruc JD, et al. (2017). Interval dosing with the HDAC inhibitor vorinostat effectively reverses HIV latency. J. Clin. Investig 127, 3126–3135. 10.1172/JCI92684. [PubMed: 28714868]
5. Archin NM, Liberty AL, Kashuba AD, Choudhary SK, Kuruc JD, Crooks AM, Parker DC, Anderson EM, Kearney MF, Strain MC, et al. (2012). Administration of vorinostat disrupts HIV-1 latency in patients on antiretroviral therapy. Nature 487, 482–485. 10.1038/nature11286. [PubMed: 22837004]
6. Søgaard OS, Graversen ME, Leth S, Olesen R, Brinkmann CR, Nissen SK, Kjaer AS, Schleimann MH, Denton PW, Hey-Cunningham WJ, et al. (2015). The Depsipeptide Romidepsin Reverses

HIV-1 Latency In Vivo. PLOS Pathog. 11, e1005142. 10.1371/journal.ppat.1005142. [PubMed: 26379282]

7. Rasmussen TA, Tolstrup M, Brinkmann CR, Olesen R, Erikstrup C, Solomon A, Winckelmann A, Palmer S, Dinarello C, Buzon M, et al. (2014). Panobinostat, a histone deacetylase inhibitor, for latent-virus reactivation in HIV-infected patients on suppressive antiretroviral therapy: a phase 1/2, single group, clinical trial. Lancet HIV 1, e13–e21. 10.1016/S2352-3018(14)70014-1. [PubMed: 26423811]
8. Leth S, Schleimann MH, Nissen SK, Højen JF, Olesen R, Graversen ME, Jørgensen S, Kjær AS, Denton PW, Mørk A, et al. (2016). Combined effect of Vacc-4x, recombinant human granulocyte macrophage colony-stimulating factor vaccination, and romidepsin on the HIV-1 reservoir (REDUC): a single-arm, phase 1B/2A trial. Lancet HIV 3, e463–e472. 10.1016/S2352-3018(16)30055-8. [PubMed: 27658863]
9. Vibholm LK, Konrad CV, Schleimann MH, Frattari G, Winckelmann A, Klastrup V, Jensen NM, Jensen SS, Schmidt M, Wittig B, et al. (2019). Effects of 24-week Toll-like receptor 9 agonist treatment in HIV type 1+ individuals. AIDS 33, 1315–1325. 10.1097/QAD.0000000000002213. [PubMed: 30932955]
10. Li JZ, Etemad B, Ahmed H, Aga E, Bosch RJ, Mellors JW, Kuritzkes DR, Lederman MM, Para M, and Gandhi RT (2016). The size of the expressed HIV reservoir predicts timing of viral rebound after treatment interruption. AIDS 30, 343–353. 10.1097/QAD.0000000000000953. [PubMed: 26588174]
11. Li JZ, Melberg M, Kittilson A, Abdel-Mohsen M, Li Y, Aga E, Bosch RJ, Wonderlich ER, Kinslow J, Giron LB, et al. (2024). Predictors of HIV rebound differ by timing of antiretroviral therapy initiation. JCI Insight 9, e173864. 10.1172/jci.insight.173864. [PubMed: 38329130]
12. Williams JP, Hurst J, Stöhr W, Robinson N, Brown H, Fisher M, Kinloch S, Cooper D, Schechter M, Tambussi G, et al. (2014). HIV-1 DNA predicts disease progression and post-treatment virological control. eLife 3, e03821. 10.7554/eLife.03821. [PubMed: 25217531]
13. Shelton EM, Reeves DB, and Bender Ignacio RA (2020). Initiation of Antiretroviral Therapy during Primary HIV Infection: Effects on the Latent HIV Reservoir, Including on Analytic Treatment Interruptions. AIDS Rev. 23, 28–39. 10.24875/AIDSRev.20000001. [PubMed: 33105471]
14. Chun TW, Justement JS, Murray D, Hallahan CW, Maenza J, Collier AC, Sheth PM, Kaul R, Ostrowski M, Moir S, et al. (2010). Rebound of plasma viremia following cessation of antiretroviral therapy despite profoundly low levels of HIV reservoir: implications for eradication. AIDS 24, 2803–2808. 10.1097/QAD.0b013e328340a239. [PubMed: 20962613]
15. Assoumou L, Weiss L, Piketty C, Burgard M, Melard A, Girard PM, Rouzioux C, and Costagliola D; ANRS 116 SALTO study group (2015). A low HIV-DNA level in peripheral blood mononuclear cells at antiretroviral treatment interruption predicts a higher probability of maintaining viral control. AIDS 29, 2003–2007. 10.1097/QAD.0000000000000734. [PubMed: 26355572]
16. Sneller MC, Justement JS, Gittens KR, Petrone ME, Clarridge KE, Proschan MA, Kwan R, Shi V, Blazkova J, Refsland EW, et al. (2017). A randomized controlled safety/efficacy trial of therapeutic vaccination in HIV-infected individuals who initiated antiretroviral therapy early in infection. Sci. Transl. Med 9, eaan8848. 10.1126/scitranslmed.aan8848. [PubMed: 29212716]
17. Pasternak AO, Grijsen ML, Wit FW, Bakker M, Jurriaans S, Prins JM, and Berkhout B (2020). Cell-associated HIV-1 RNA predicts viral rebound and disease progression after discontinuation of temporary early ART. Insight 5. Art. JCI 10.1172/jci.insight.134196.
18. Bruner KM, Wang Z, Simonetti FR, Bender AM, Kwon KJ, SenGupta S, Fray EJ, Beg SA, Antar AAR, Jenike KM, et al. (2019). A quantitative approach for measuring the reservoir of latent HIV-1 proviruses. Nature 566, 120–125. 10.1038/s41586-019-0898-8. [PubMed: 30700913]
19. SenGupta D, Brinson C, DeJesus E, Mills A, Shalit P, Guo S, Cai Y, Wallin JJ, Zhang L, Humeniuk R, et al. (2021). The TLR7 agonist vesatolimod induced a modest delay in viral rebound in HIV controllers after cessation of antiretroviral therapy. Sci. Transl. Med 13, eabg3071. 10.1126/scitranslmed.abg3071. [PubMed: 34162752]

20. Etemad B, Sun X, Li Y, Melberg M, Moisi D, Gottlieb R, Ahmed H, Aga E, Bosch RJ, Acosta EP, et al. (2023). HIV post-treatment controllers have distinct immunological and virological features. Proc. Natl. Acad. Sci. USA 120, e2218960120. 10.1073/pnas.2218960120.
21. Giron LB, Palmer CS, Liu Q, Yin X, Papasavvas E, Sharaf R, Etemad B, Damra M, Goldman AR, Tang HY, et al. (2021). Non-invasive plasma glycomic and metabolic biomarkers of post-treatment control of HIV. Nat. Commun 12, 3922. 10.1038/s41467-021-24077-w. [PubMed: 34188039]
22. Wedrychowski A, Martin HA, Li Y, Telwatte S, Kadiyala GN, Melberg M, Etemad B, Connick E, Jacobson JM, Margolis DM, et al. (2023). Transcriptomic Signatures of Human Immunodeficiency Virus Post-Treatment Control. J. Virol 97, e0125422. 10.1128/jvi.01254-22. [PubMed: 36541802]
23. Kearney MF, Wiegand A, Shao W, Coffin JM, Mellors JW, Lederman M, Gandhi RT, Keele BF, and Li JZ (2016). Origin of Rebound Plasma HIV Includes Cells with Identical Proviruses That Are Transcriptionally Active before Stopping of Antiretroviral Therapy. J. Virol 90, 1369–1376. 10.1128/JVI.02139-15. [PubMed: 26581989]
24. Prigann J, Tavora R, Furler O'Brien RLF, Schulze-Gahmen U, Boehm D, Roan NR, Nixon DF, Ndhlovu LC, Valente S, and Ott M (2024). Silencing the transcriptionally active HIV reservoir to improve treatment outcomes. Nat. Microbiol 9, 2470–2472. 10.1038/s41564-024-01816-5. [PubMed: 39289508]
25. Hurst J, Hoffmann M, Pace M, Williams JP, Thornhill J, Hamlyn E, Meyerowitz J, Willberg C, Koelsch KK, Robinson N, et al. (2015). Immunological biomarkers predict HIV-1 viral rebound after treatment interruption. Nat. Commun 6, 8495. 10.1038/ncomms9495. [PubMed: 26449164]
26. Cavrois M, Banerjee T, Mukherjee G, Raman N, Hussien R, Rodriguez BA, Vasquez J, Spitzer MH, Lazarus NH, Jones JJ, et al. (2017). Mass Cytometric Analysis of HIV Entry, Replication, and Remodeling in Tissue CD4+ T Cells. Cell Rep. 20, 984–998. 10.1016/j.celrep.2017.06.087. [PubMed: 28746881]
27. Ma T, Luo X, George AF, Mukherjee G, Sen N, Spitzer TL, Giudice LC, Greene WC, and Roan NR (2020). HIV efficiently infects T cells from the endometrium and remodels them to promote systemic viral spread. eLife 9, e55487. 10.7554/eLife.55487. [PubMed: 32452381]
28. Vendrame E, McKechnie JL, Ranganath T, Zhao NQ, Rustagi A, Vergara R, Ivison GT, Kronstad LM, Simpson LJ, and Blish CA (2020). Profiling of the Human Natural Killer Cell Receptor-Ligand Repertoire. J. Vis. Exp 165. 10.3791/61912.
29. Vendrame E, Seiler C, Ranganath T, Zhao NQ, Vergara R, Alary M, Labbé AC, Guédou F, Poudrier J, Holmes S, et al. (2020). TIGIT is upregulated by HIV-1 infection and marks a highly functional adaptive and mature subset of natural killer cells. AIDS 34, 801–813. 10.1097/QAD.0000000000002488. [PubMed: 32028328]
30. Blondel VD, Guillaume JL, Lambiotte R, and Lefebvre E (2008). Fast unfolding of communities in large networks. J. Stat. Mech 2008, P10008. 10.1088/1742-5468/2008/10/P10008.
31. Gattinoni L, Lugli E, Ji Y, Pos Z, Paulos CM, Quigley MF, Almeida JR, Gostick E, Yu Z, Carpenito C, et al. (2011). A human memory T cell subset with stem cell-like properties. Nat. Med 17, 1290–1297. 10.1038/nm.2446. [PubMed: 21926977]
32. Lopez-Vergès S, Milush JM, Pandey S, York VA, Arakawa-Hoyt J, Pircher H, Norris PJ, Nixon DF, and Lanier LL (2010). CD57 defines a functionally distinct population of mature NK cells in the human CD56dimCD16+ NK-cell subset. Blood 116, 3865–3874. 10.1182/blood-2010-04-282301. [PubMed: 20733159]
33. Hu PF, Hultin LE, Hultin P, Hausner MA, Hirji K, Jewett A, Bonavida B, Detels R, and Giorgi JV (1995). Natural killer cell immunodeficiency in HIV disease is manifest by profoundly decreased numbers of CD16+CD56+ cells and expansion of a population of CD16dimCD56- cells with low lytic activity. J. Acquir. Immune Defic. Syndr. Hum. Retrovirol 10, 331–340. 10.1097/00042560-199511000-00005. [PubMed: 7552495]
34. Bradley T, Peppa D, Pedroza-Pacheco I, Li D, Cain DW, Henao R, Venkat V, Hora B, Chen Y, Vandergrift NA, et al. (2018). RAB11FIP5 Expression and Altered Natural Killer Cell Function Are Associated with Induction of HIV Broadly Neutralizing Antibody Responses. Cell 175, 387–399.e17. 10.1016/j.cell.2018.08.064. [PubMed: 30270043]
35. Cocker ATH, Guethlein LA, and Parham P (2023). The CD56-CD16+ NK cell subset in chronic infections. Biochem. Soc. Trans 51, 1201–1212. 10.1042/BST20221374. [PubMed: 37140380]

36. Stuart T, Butler A, Hoffman P, Hafemeister C, Papalexi E, Mauck WM 3rd, Hao Y, Stoeckius M, Smibert P, and Satija R (2019). Comprehensive Integration of Single-Cell Data. Cell 177, 1888–1902.e21. 10.1016/j.cell.2019.05.031. [PubMed: 31178118]
37. Collora JA, Liu R, Pinto-Santini D, Ravindra N, Ganoza C, Lama JR, Alfaro R, Chiarella J, Spudich S, Mounzer K, et al. (2022). Single-cell multiomics reveals persistence of HIV-1 in expanded cytotoxic T cell clones. Immunity 55, 1013–1031.e7. 10.1016/j.immuni.2022.03.004. [PubMed: 35320704]
38. Dwivedi AK, Gornalusse GG, Siegel DA, Barbehenn A, Thanh C, Hoh R, Hobbs KS, Pan T, Gibson EA, Martin J, et al. (2023). A cohort-based study of host gene expression: tumor suppressor and innate immune/inflammatory pathways associated with the HIV reservoir size. PLOS Pathog. 19, e1011114. 10.1371/journal.ppat.1011114. [PubMed: 38019897]
39. Brugarolas J, Lei K, Hurley RL, Manning BD, Reiling JH, Hafen E, Witters LA, Ellisen LW, and Kaelin WG Jr. (2004). Regulation of mTOR function in response to hypoxia by REDD1 and the TSC1/TSC2 tumor suppressor complex. Genes Dev. 18, 2893–2904. 10.1101/gad.1256804. [PubMed: 15545625]
40. Planas D, Zhang Y, Monteiro P, Goulet JP, Gosselin A, Grandvaux N, Hope TJ, Fassati A, Routy JP, and Ancuta P (2017). HIV-1 selectively targets gut-homing CCR6+CD4+ T cells via mTOR-dependent mechanisms. JCI Insight 2, e93230. 10.1172/jci.insight.93230. [PubMed: 28768913]
41. Henrich TJ, Schreiner C, Cameron C, Hogan LE, Richardson B, Rutishauser RL, Deitchman AN, Chu S, Rogers R, Thanh C, et al. (2021). Everolimus, an mTORC1/2 inhibitor, in ART-suppressed individuals who received solid organ transplantation: A prospective study. Am. J. Transplant 21, 1765–1779. 10.1111/ajt.16244. [PubMed: 32780519]
42. Besnard E, Hakre S, Kampmann M, Lim HW, Hosmane NN, Martin A, Bassik MC, Verschueren E, Battivelli E, Chan J, et al. (2016). The mTOR Complex Controls HIV Latency. Cell Host Microbe 20, 785–797. 10.1016/j.chom.2016.11.001. [PubMed: 27978436]
43. Gramatica A, Schwarzer R, Brantley W, Varco-Merth B, Sperber HS, Hull PA, Montano M, Migueles SA, Rosenthal D, Hogan LE, et al. (2021). Evaluating a New Class of AKT/mTOR Activators for HIV Latency Reversing Activity Ex Vivo and In Vivo. J. Virol 95, e02393–20. 10.1128/JVI.02393-20. [PubMed: 33536176]
44. Lassen KG, Hebbeler AM, Bhattacharyya D, Lobritz MA, and Greene WC (2012). A flexible model of HIV-1 latency permitting evaluation of many primary CD4 T-cell reservoirs. PLOS One 7, e30176. 10.1371/journal.pone.0030176. [PubMed: 22291913]
45. Ben Sahra I, Regazzetti C, Robert G, Laurent K, Le Marchand-Brustel Y, Auberger P, Tanti JF, Giorgetti-Peraldi S, and Bost F (2011). Metformin, independent of AMPK, induces mTOR inhibition and cell-cycle arrest through REDD1. Cancer Res. 71, 4366–4372. 10.1158/0008-5472.CAN-10-1769. [PubMed: 21540236]
46. Shikuma CM, Chew GM, Kohorn L, Souza SA, Chow D, SahBandar IN, Park EY, Hanks N, Gangcuangco LMA, Gerschenson M, et al. (2020). Short Communication: Metformin Reduces CD4 T Cell Exhaustion in HIV-Infected Adults on Suppressive Antiretroviral Therapy. AIDS Res. Hum. Retrovir 36, 303–305. 10.1089/AID.2019.0078. [PubMed: 31731885]
47. Corley MJ, Pang APS, Shikuma CM, and Ndhlovu LC (2024). Cell-type specific impact of metformin on monocyte epigenetic age reversal in virally suppressed older people living with HIV. Aging Cell 23, e13926. 10.1111/acel.13926. [PubMed: 37675817]
48. Hsiao F, Frouard J, Gramatica A, Xie G, Telwatte S, Lee GQ, Roychoudhury P, Schwarzer R, Luo X, Yukl SA, et al. (2020). Tissue memory CD4+ T cells expressing IL-7 receptor-alpha (CD127) preferentially support latent HIV-1 infection. PLOS Pathog. 16, e1008450. 10.1371/journal.ppat.1008450. [PubMed: 32353080]
49. Garcia JV, and Miller AD (1991). Serine phosphorylation-independent downregulation of cell-surface CD4 by nef. Nature 350, 508–511. 10.1038/350508a0. [PubMed: 2014052]
50. Frouard J, Telwatte S, Luo X, Gill N, Thomas R, Arneson D, Roychoudhury P, Butte AJ, Wong JK, Hoh R, et al. (2026). HIV-seq reveals gene expression differences between HIV-transcribing cells from viremic and suppressed people with HIV. Nat Commun 17. 10.1038/s41467-026-68797-3.
51. Krasnopolsky S, Kuzmina A, and Taube R (2020). Genome-wide CRISPR knockout screen identifies ZNF304 as a silencer of HIV transcription that promotes viral latency. PLOS Pathog. 16, e1008834. 10.1371/journal.ppat.1008834. [PubMed: 32956422]

52. Yang B, Fang L, Gao Q, Xu C, Xu J, Chen ZX, Wang Y, and Yang P (2022). Species-specific KRAB-ZFPs function as repressors of retroviruses by targeting PBS regions. Proc. Natl. Acad. Sci. USA 119, e2119415119. 10.1073/pnas.2119415119.

53. Nishitsuji H, Sawada L, Sugiyama R, and Takaku H (2015). ZNF10 inhibits HIV-1 LTR activity through interaction with NF-κB and Sp1 binding motifs. FEBS Lett. 589, 2019–2025. 10.1016/j.febslet.2015.06.013. [PubMed: 26096782]

54. Nishitsuji H, Abe M, Sawada R, and Takaku H (2012). ZBRK1 represses HIV-1 LTR-mediated transcription. FEBS Lett. 586, 3562–3568. 10.1016/j.febslet.2012.08.010. [PubMed: 22975076]

55. Singh M, Leddy SM, Iñiguez LP, Bendall ML, Nixon DF, and Feschotte C (2025). Transposable elements may enhance antiviral resistance in HIV-1 elite controllers. Genome Biol. 26, 28. 10.1186/s13059-025-03484-y. [PubMed: 39988678]

56. Tapia G, Højen JF, Ökvist M, Olesen R, Leth S, Nissen SK, VanBelzen DJ, O'Doherty U, Mørk A, Krogsgaard K, et al. (2017). Sequential Vacc-4x and romidepsin during combination antiretroviral therapy (cART): Immune responses to Vacc-4x regions on p24 and changes in HIV reservoirs. J. Infect 75, 555–571. 10.1016/j.jinf.2017.09.004. [PubMed: 28917661]

57. Scott-Algara D, Arnold V, Didier C, Kattan T, Pirozzi G, Barré-Sinoussi F, and Pancino G (2008). The CD85j+ NK cell subset potently controls HIV-1 replication in autologous dendritic cells. PLOS One 3, e1975. 10.1371/journal.pone.0001975. [PubMed: 18398485]

58. Song J, So T, Cheng M, Tang X, and Croft M (2005). Sustained survivin expression from OX40 costimulatory signals drives T cell clonal expansion. Immunity 22, 621–631. 10.1016/j.immuni.2005.03.012. [PubMed: 15894279]

59. Mutascio S, Mota T, Franchitti L, Sharma AA, Willemse A, Bergstresser SN, Wang H, Statzu M, Tharp GK, Weiler J, et al. (2023). CD8+ T cells promote HIV latency by remodeling CD4+ T cell metabolism to enhance their survival, quiescence, and stemness. Immunity 56, 1132–1147.e6. 10.1016/j.immuni.2023.03.010. [PubMed: 37030290]

60. Cepek KL, Shaw SK, Parker CM, Russell GJ, Morrow JS, Rimm DL, and Brenner MB (1994). Adhesion between epithelial cells and T lymphocytes mediated by E-cadherin and the alpha E beta 7 integrin. Nature 372, 190–193. 10.1038/372190a0. [PubMed: 7969453]

61. Yukl SA, Khan S, Chen TH, Trapecar M, Wu F, Xie G, Telwatte S, Fulop D, Pico AR, Laird GM, et al. (2020). Shared Mechanisms Govern HIV Transcriptional Suppression in Circulating CD103(+) and Gut CD4(+) T Cells. J. Virol 95, e01331–20. 10.1128/JVI.01331-20. [PubMed: 33115867]

62. Jimenez-Leon MR, Gasca-Capote C, Roca-Oporto C, Espinosa N, Sobrino S, Fontillon-Alberdi M, Gao C, Roseto I, Gladkov G, Rivas-Jeremias I, et al. (2024). Vedolizumab and ART in recent HIV-1 infection unveil the role of α4β7 in reservoir size. JCI Insight 9, e182312. 10.1172/jci.insight.182312. [PubMed: 38980725]

63. Guo H, Wang Q, Ghneim K, Wang L, Rampanelli E, Holley-Guthrie E, Cheng L, Garrido C, Margolis DM, Eller LA, et al. (2021). Multi-omics analyses reveal that HIV-1 alters CD4+ T cell immunometabolism to fuel virus replication. Nat. Immunol 22, 423–433. 10.1038/s41590-021-00898-1. [PubMed: 33767427]

64. Fert A, Richard J, Raymond Marchand L, Planas D, Routy JP, Chomont N, Finzi A, and Ancuta P (2024). Metformin facilitates viral reservoir reactivation and their recognition by anti-HIV-1 envelope antibodies. iScience 27, 110670. 10.1016/j.isci.2024.110670. [PubMed: 39252967]

65. Chew GM, Padua AJP, Chow DC, Souza SA, Clements DM, Corley MJ, Pang APS, Alejandria MM, Gerschenson M, Shikuma CM, et al. (2021). Effects of Brief Adjunctive Metformin Therapy in Virologically Suppressed HIV-Infected Adults on Polyfunctional HIV-Specific CD8 T Cell Responses to PD-L1 Blockade. AIDS Res. Hum. Retrovir 37, 24–33. 10.1089/AID.2020.0172. [PubMed: 33019813]

66. Planas D, Pagliuzza A, Ponte R, Fert A, Marchand LR, Massanella M, Gosselin A, Mehraj V, Dupuy FP, Isnard S, et al. (2021). LILAC pilot study: Effects of metformin on mTOR activation and HIV reservoir persistence during antiretroviral therapy. EBiomedicine 65, 103270. 10.1016/j.ebiom.2021.103270. [PubMed: 33662832]

67. Lian X, Seiger KW, Parsons EM, Gao C, Sun W, Gladkov GT, Roseto IC, Einkauf KB, Osborn MR, Chevalier JM, et al. (2023). Progressive transformation of the HIV-1 reservoir

cell profile over two decades of antiviral therapy. Cell Host Microbe 31, 83–96.e5. 10.1016/j.chom.2022.12.002. [PubMed: 36596305]

68. Fombellida-Lopez C, Berkhout B, Darcis G, and Pasternak AO (2024). Persistent HIV-1 transcription during ART: time to reassess its significance? Curr. Opin. HIV AIDS 19, 124–132. 10.1097/COH.0000000000000849. [PubMed: 38502547]
69. Hatano H, Jain V, Hunt PW, Lee TH, Sinclair E, Do TD, Hoh R, Martin JN, McCune JM, Hecht F, et al. (2013). Cell-based measures of viral persistence are associated with immune activation and programmed cell death protein 1 (PD-1)-expressing CD4+ T cells. J. Infect. Dis 208, 50–56. 10.1093/infdis/jis630. [PubMed: 23089590]
70. Olson A, Coote C, Snyder-Cappione JE, Lin N, and Sagar M (2021). HIV-1 Transcription but Not Intact Provirus Levels are Associated With Systemic Inflammation. J. Infect. Dis 223, 1934–1942. 10.1093/infdis/jiaa657. [PubMed: 33075121]
71. Scherpenisse M, Kootstra NA, Bakker M, Berkhout B, and Pasternak AO (2021). Cell-Associated HIV-1 Unspliced-to-Multiply-Spliced RNA Ratio at 12 Weeks of ART Predicts Immune Reconstitution on Therapy. mBio 12, e00099–21. 10.1128/mBio.00099-21. [PubMed: 33688002]
72. Reeves DB, Gaebler C, Oliveira TY, Peluso MJ, Schiffer JT, Cohn LB, Deeks SG, and Nussenzweig MC (2023). Impact of misclassified defective proviruses on HIV reservoir measurements. Nat. Commun 14, 4186. 10.1038/s41467-023-39837-z. [PubMed: 37443365]
73. Olesen R, Vigano S, Rasmussen TA, Søgaard OS, Ouyang Z, Buzon M, Bashirova A, Carrington M, Palmer S, Brinkmann CR, et al. (2015). Innate Immune Activity Correlates with CD4 T Cell-Associated HIV-1 DNA Decline during Latency-Reversing Treatment with Panobinostat. J. Virol 89, 10176–10189. 10.1128/JVI.01484-15. [PubMed: 26223643]
74. Høgh Kølbæk Kjær AS, Brinkmann CR, Dinarello CA, Olesen R, Østergaard L, Søgaard OS, Tolstrup M, and Rasmussen TA (2015). The histone deacetylase inhibitor panobinostat lowers biomarkers of cardiovascular risk and inflammation in HIV patients. AIDS 29, 1195–1200. 10.1097/QAD.0000000000000678. [PubMed: 25870990]
75. Vibholm L, Schleimann MH, Højen JF, Benfield T, Offersen R, Rasmussen K, Olesen R, Dige A, Agnholt J, Grau J, et al. (2017). Short-Course Toll-Like Receptor 9 Agonist Treatment Impacts Innate Immunity and Plasma Viremia in Individuals With Human Immunodeficiency Virus Infection. Clin. Infect. Dis 64, 1686–1695. 10.1093/cid/cix201. [PubMed: 28329286]
76. Butler A, Hoffman P, Smibert P, Papalexi E, and Satija R (2018). Integrating single-cell transcriptomic data across different conditions, technologies, and species. Nat. Biotechnol 36, 411–420. 10.1038/nbt.4096. [PubMed: 29608179]
77. Hao Y, Hao S, Andersen-Nissen E, Mauck WM 3rd, Zheng S, Butler A, Lee MJ, Wilk AJ, Darby C, Zager M, et al. (2021). Integrated analysis of multimodal single-cell data. Cell 184, 3573–3587.e29. 10.1016/j.cell.2021.04.048. [PubMed: 34062119]
78. Hao Y, Stuart T, Kowalski MH, Choudhary S, Hoffman P, Hartman A, Srivastava A, Molla G, Madad S, Fernandez-Granda C, et al. (2024). Dictionary learning for integrative, multimodal and scalable single-cell analysis. Nat. Biotechnol 42, 293–304. 10.1038/s41587-023-01767-y. [PubMed: 37231261]
79. Satija R, Farrell JA, Gennert D, Schier AF, and Regev A (2015). Spatial reconstruction of single-cell gene expression data. Nat. Biotechnol 33, 495–502. 10.1038/nbt.3192. [PubMed: 25867923]
80. Becht E, McInnes L, Healy J, Dutertre CA, Kwok IWH, Ng LG, Ginhoux F, and Newell EW (2018). Dimensionality reduction for visualizing single-cell data using UMAP. Nat. Biotechnol 10.1038/nbt.4314.
81. Korsunsky I, Millard N, Fan J, Slowikowski K, Zhang F, Wei K, Baglaenko Y, Brenner M, Loh PR, and Raychaudhuri S (2019). Fast, sensitive and accurate integration of single-cell data with Harmony. Nat. Methods 16, 1289–1296. 10.1038/s41592-019-0619-0. [PubMed: 31740819]
82. Breiman L (2001). Random Forests. Mach. Learn 45, 5–32. 10.1023/A:1010933404324.
83. George AF, Luo X, Neidleman J, Hoh R, Vohra P, Thomas R, Shin MG, Lee MJ, Blish CA, Deeks SG, et al. (2022). Deep Phenotypic Analysis of Blood and Lymphoid T and NK Cells From HIV+ Controllers and ART-Suppressed Individuals. Front. Immunol 13, 803417. 10.3389/fimmu.2022.803417. [PubMed: 35154118]

84. Yin K, Peluso MJ, Luo X, Thomas R, Shin MG, Neidleman J, Andrew A, Young KC, Ma T, Hoh R, et al. (2024). Long COVID manifests with T cell dysregulation, inflammation and an uncoordinated adaptive immune response to SARS-CoV-2. Nat. Immunol 25, 218–225. 10.1038/s41590-023-01724-6. [PubMed: 38212464]
85. Bates D, Mächler M, Bolker B, and Walker S (2015). Fitting Linear Mixed-Effects Models Using lme4. J. Stat. Softw 67, 1–48. 10.18637/jss.v067.i01.
86. Lenth R (2024) Emmeans: Estimated Marginal Means, Aka Least-Squares Means.
87. Burbelo PD, Ching KH, Klimavicz CM, and Iadarola MJ (2009). Antibody profiling by Luciferase Immunoprecipitation Systems (LIPS). J. Vis. Exp 32, 1549. 10.3791/1549.
88. Feng W, Beer JC, Hao Q, Ariyapala IS, Sahajan A, Komarov A, Cha K, Moua M, Qiu X, Xu X, et al. (2023). NULISA: a proteomic liquid biopsy platform with attomolar sensitivity and high multiplexing. Nat. Commun 14, 7238. 10.1038/s41467-023-42834-x. [PubMed: 37945559]
89. Patel H, Ewels P, Manning J, Garcia MU, Peltzer A, Hammarén R, Botvinnik O, Talbot A, Sturm G, nf-core bot, et al. (2024). nf-core/rnaseq: nf-core/rnaseq v3.16.0 - Fire Ferret (3.16.0). (Zenodo). 10.5281/zenodo.13882081.
90. Aronesty E (2011) EA-Utils: Command-Line Tools for Processing Biological Sequencing Data.
91. Krueger F (2019). Trim Galore. A wrapper tool around Cutadapt and FastQC to consistently apply quality and adapter trimming to FastQ files. https://www.bioinformatics.babraham.ac.uk/projects/trim_galore.
92. Andrews S (2023). FastQC: a quality control tool for high throughput sequence data. http://www.bioinformatics.babraham.ac.uk/projects/fastqc.
93. Wang L, Wang S, and Li W (2012). RSeQC: quality control of RNA-seq experiments. Bioinformatics 28, 2184–2185. 10.1093/bioinformatics/bts356. [PubMed: 22743226]
94. Dobin A, Davis CA, Schlesinger F, Drenkow J, Zaleski C, Jha S, Batut P, Chaisson M, and Gingeras TR (2013). STAR: ultrafast universal RNA-seq aligner. Bioinformatics 29, 15–21. 10.1093/bioinformatics/bts635. [PubMed: 23104886]
95. Liao Y, Smyth GK, and Shi W (2014). featureCounts: an efficient general purpose program for assigning sequence reads to genomic features. Bioinformatics 30, 923–930. 10.1093/bioinformatics/btt656. [PubMed: 24227677]
96. Patro R, Duggal G, Love MI, Irizarry RA, and Kingsford C (2017). Salmon provides fast and bias-aware quantification of transcript expression. Nat. Methods 14, 417–419. 10.1038/nmeth.4197. [PubMed: 28263959]
97. Soneson C, Love MI, and Robinson MD (2015). Differential analyses for RNA-seq: transcript-level estimates improve gene-level inferences. F1000Res 4, 1521. 10.12688/f1000research.7563.2. [PubMed: 26925227]
98. Robinson MD, McCarthy DJ, and Smyth GK (2010). edgeR: a Bioconductor package for differential expression analysis of digital gene expression data. Bioinformatics 26, 139–140. 10.1093/bioinformatics/btp616. [PubMed: 19910308]
99. Lun ATL, Chen Y, and Smyth GK (2016). It's DE-licious: A Recipe for Differential Expression Analyses of RNA-seq Experiments Using Quasi-Likelihood Methods in edgeR. Methods Mol. Biol 1418, 391–416. 10.1007/978-1-4939-3578-9_19. [PubMed: 27008025]
100. Blighe K, Rana S, and Lewis M (2018). EnhancedVolcano: Publication-ready volcano plots with enhanced colouring and labeling. https://github.com/kevinblighe/EnhancedVolcano.
101. Gene Ontology Consortium, Aleksander SA, Balhoff J, Carbon S, Cherry JM, Drabkin HJ, Ebert D, Feuermann M, Gaudet P, Harris NL, et al. (2023). The Gene Ontology knowledgebase in 2023. Genetics 224, iyad031. 10.1093/genetics/iyad031. [PubMed: 36866529]
102. Ashburner M, Ball CA, Blake JA, Botstein D, Butler H, Cherry JM, Davis AP, Dolinski K, Dwight SS, Eppig JT, et al. (2000). Gene ontology: tool for the unification of biology. The Gene Ontology Consortium. Nat. Genet 25, 25–29. 10.1038/75556. [PubMed: 10802651]
103. Martens M, Ammar A, Riutta A, Waagmeester A, Slenter DN, Hanspers K, A Miller R, Digles D, Lopes EN, Ehrhart F, et al. (2021). WikiPathways: connecting communities. Nucleic Acids Res. 49, D613–D621. 10.1093/nar/gkaa1024. [PubMed: 33211851]

104. Yu G, Wang LG, Han Y, and He QY (2012). clusterProfiler: an R package for comparing biological themes among gene clusters. Omics 16, 284–287. 10.1089/omi.2011.0118. [PubMed: 22455463]

105. Schmiedel BJ, Singh D, Madrigal A, Valdovino-Gonzalez AG, White BM, Zapardiel-Gonzalo J, Ha B, Altay G, Greenbaum JA, McVicker G, et al. (2018). Impact of Genetic Polymorphisms on Human Immune Cell Gene Expression. Cell 175, 1701–1715.e16. 10.1016/j.cell.2018.10.022. [PubMed: 30449622]

106. Monaco G, Lee B, Xu W, Mustafah S, Hwang YY, Carré C, Burdin N, Visan L, Ceccarelli M, Poidinger M, et al. (2019). RNA-Seq Signatures Normalized by mRNA Abundance Allow Absolute Deconvolution of Human Immune Cell Types. Cell Rep. 26, 1627–1640.e7. 10.1016/j.celrep.2019.01.041. [PubMed: 30726743]

107. Chan JK, Bhattacharyya D, Lassen KG, Ruelas D, and Greene WC (2013). Calcium/calcineurin synergizes with prostratin to promote NF-κB dependent activation of latent HIV. PLOS One 8, e77749. 10.1371/journal.pone.0077749. [PubMed: 24204950]

108. Ashokkumar M, Hafer TL, Felton A, Archin NM, Margolis DM, Emerman M, and Browne EP (2025). A targeted CRISPR screen identifies ETS1 as a regulator of HIV-1 latency. PLOS Pathog. 21, e1012467. 10.1371/journal.ppat.1012467. [PubMed: 40198713]

109. Imbeault M, Helleboid PY, and Trono D (2017). KRAB zinc-finger proteins contribute to the evolution of gene regulatory networks. Nature 543, 550–554. 10.1038/nature21683. [PubMed: 28273063]

110. Jordan A, Bisgrove D, and Verdin E (2003). HIV reproducibly establishes a latent infection after acute infection of T cells in vitro. EMBO J. 22, 1868–1877. 10.1093/emboj/cdg188. [PubMed: 12682019]

111. Shan L, Yang HC, Rabi SA, Bravo HC, Shroff NS, Irizarry RA, Zhang H, Margolick JB, Siliciano JD, and Siliciano RF (2011). Influence of host gene transcription level and orientation on HIV-1 latency in a primary-cell model. J. Virol 85, 5384–5393. 10.1128/JVI.02536-10. [PubMed: 21430059]

112. Benjamini Y, and Hochberg Y (1995). Controlling the False Discovery Rate: A Practical and Powerful Approach to Multiple Testing. J.R. Stat. Soc. Series B Methodol 57, 289–300. http://www.jstor.org/stable/2346101.

113. Belsley DA, Kuh E, and Welsch RE (2005). Regression Diagnostics: Identifying Influential Data and Sources of Collinearity (John Wiley & Sons). 10.1002/0471725153.

Highlights

- "Omics" analysis of PBMCs from people with HIV (PWH) undergoing ART interruption
- Atypical NK cells, and durable/CD103^{+} T cells, associate with delayed HIV rebound
- Delayed rebound is associated with CD4^{+} T cell expression of *ZNF254* and *DDIT4*
- ZNF254, DDIT4, and metformin silence HIV gene expression

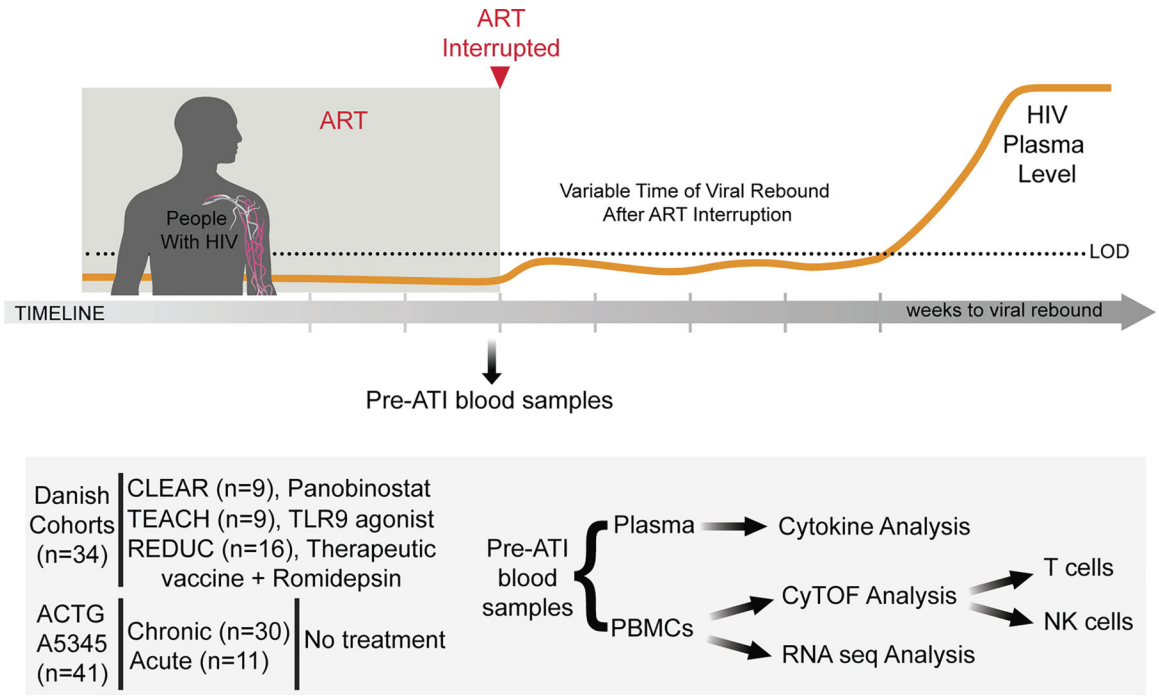

Figure 1. Schematic of experimental design

Blood collected immediately prior to ATI from three interventional cohorts (CLEAR, TEACH, and REDUC) based in Denmark, and non-interventional cohort ACTG A5345, were profiled by multiple methods including CyTOF and RNA-seq, and associated with HIV reservoir and time-to-rebound.

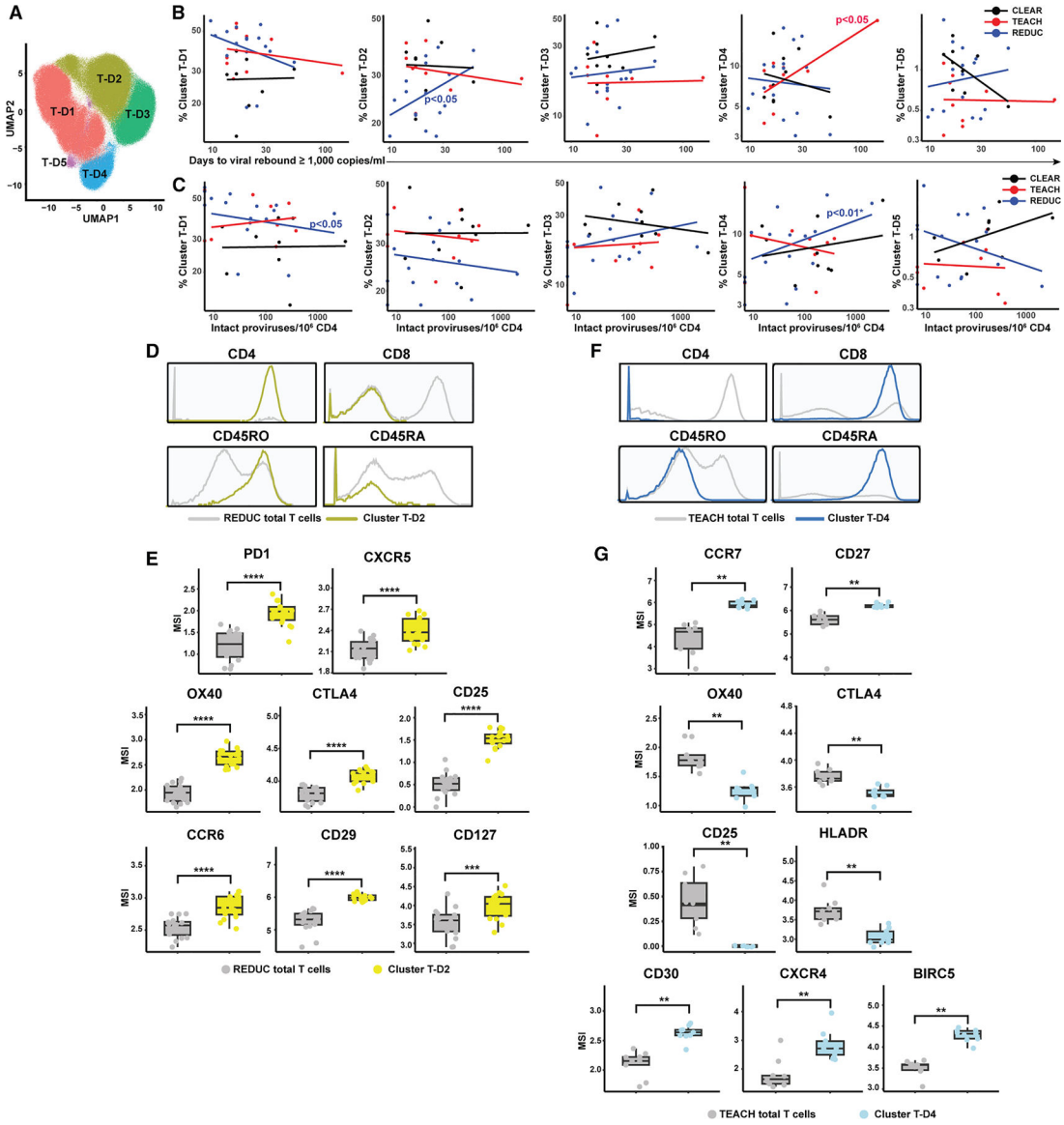

Figure 2. Clusters T-D2 and T-D4 predict increased time-to-rebound in REDUC and TEACH, respectively

(A) Uniform manifold approximation and projection (UMAP) depiction of the five clusters of T cells (T-D1 to T-D5) from CLEAR, TEACH, and REDUC.

(B and C) Association of T cell cluster frequencies with time-to-rebound to ≥ 1,000 copies/mL of HIV RNA (B) or number of intact proviruses per million $CD4^+$ T cells (C). *p*-values were calculated based on fit of the generalized linear mixed effects models (GLMM) modeling, and those highlighted with an asterisk (*) remained significant ($p < 0.05$) following adjustment for multiple comparison using the false discovery rate (FDR)-based Benjamini-Hochberg method.

(D) Histogram plots demonstrating that cluster T-D2 are primarily memory ($CD45RO^+CD45RA^-$) $CD4^+$ T cells.

(E) Phenotypic features of cluster T-D2 cells.

(F) Histogram plots demonstrating that cluster T-D4 are $CD45RO^-CD45RA^+$.

(G) Phenotypic features of cluster T-D4 cells. In (E) and (G), boxes represent the interquartile range (IQR), with horizontal lines indicating median. Individual datapoints correspond to participants. *p*-values were calculated by Wilcoxon signed-rank test and adjusted for multiple comparisons using the FDR-based Benjamini-Hochberg method. See also Figures S1, S2, and S7.

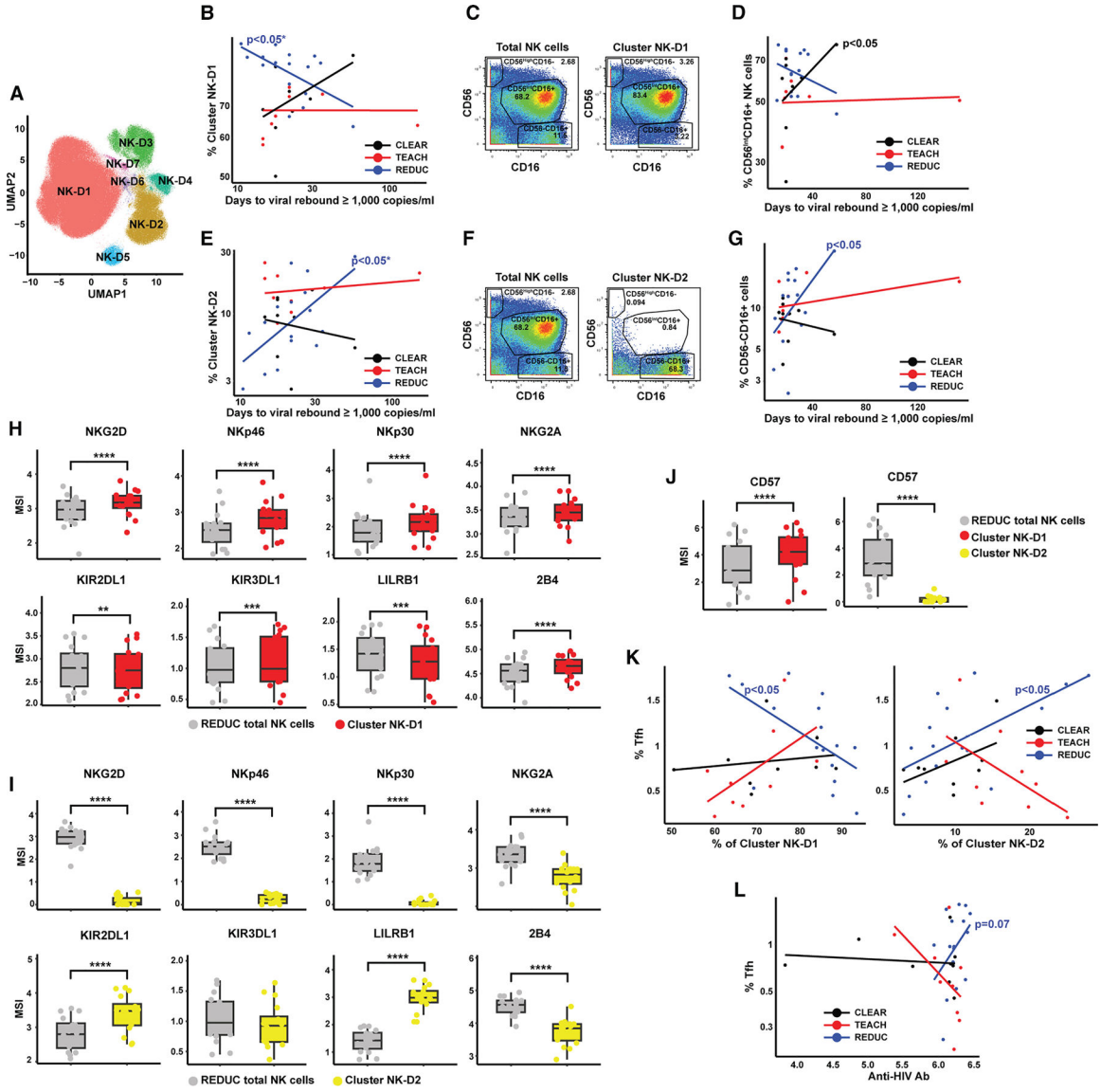

Figure 3. In REDUC, CD56^{int}CD16^{+} NK cells associate with shorter time-to-rebound, while CD56^{-}CD16^{+} NK cells associate with longer time-to-rebound

(A) UMAP depiction of the seven clusters of NK cells (NK-D1 to NK-D7) from CLEAR, TEACH, and REDUC.

(B) Association of cluster NK-D1 with time-to-rebound to ≥ 1,000 copies/mL of HIV RNA.

(C) Cluster NK-D1 are primarily CD56^{Int}CD16^{+} cells.

(D) Association of CD56^{Int}CD16^{+} NK cell frequencies with time-to-rebound to ≥ 1,000 copies/mL of HIV RNA.

(E) Association of cluster NK-D2 with time-to-rebound to ≥ 1,000 copies/mL of HIV RNA.

(F) Cluster NK-D2 are primarily CD56^{-}CD16^{+} cells.

(G) Association of CD56^{-}CD16^{+} NK cell frequencies with time-to-rebound to ≥ 1,000 copies/mL of HIV RNA.

(H and I) NK receptor expression of cluster NK-D1 (H) or NK-D2 (I) cells.

(J) CD57 expression on cluster NK-D1 and NK-D2 cells from REDUC.

(K) Associations of Tfh frequencies with cluster NK-D1 and NK-D2 frequencies.
(L) Association of Tfh frequencies with HIV serological responses. In (B), (D), (E), (G), (K), and (L), *p*values were calculated based on fit of GLMM modeling. *p*values highlighted with an asterisk (*) remained significant ($p < 0.05$) following adjustment for multiple comparison using the FDR-based Benjamini-Hochberg method. In (H)–(J), boxes represent the IQR, with horizontal lines indicating median. Individual datapoints correspond to participants. *p*values were calculated by Wilcoxon signed-rank test and adjusted for multiple comparisons using the FDR-based Benjamini-Hochberg method.
See also Figures S1, S2, and S7.

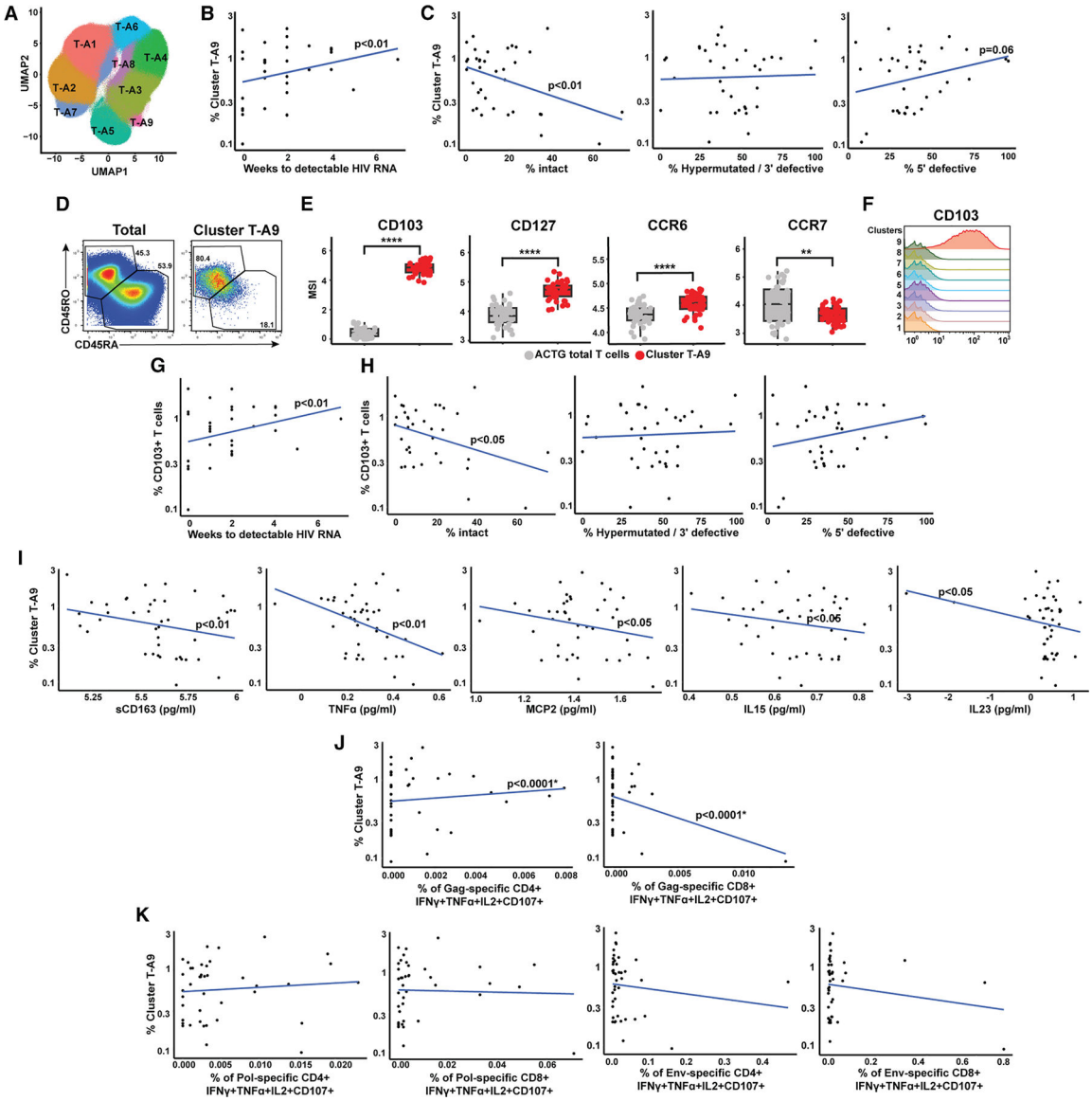

Figure 4. CD103^{+} cluster associates with increased time to initial detectable viremia in ACTG A5345

(A) UMAP depiction of the nine clusters of T cells (T-A1 to T-A9) from ACTG A5345.

(B) Association of cluster T-A9 with time-to-detectable HIV RNA.

(C) Association of cluster T-A9 with HIV reservoir.

(D) Cluster T-A9 are primarily CD45RO^{+}CD45RA^{-}.

(E) Phenotypic features of cluster T-A9 cells.

(F) CD103 is exclusively highly expressed in cluster T-A9.

(G and H) Association of CD103^{+} T cell frequencies with time-to-detectable HIV RNA (G) or HIV reservoir (H).

(I) Association of cluster T-A9 with inflammatory markers.

(J and K) Association of cluster T-A9 with frequencies of polyfunctional Gag-specific T cells (J) or pol/env-specific T cells (K). *p*values in (B), (C), and (G)–(K) were calculated based on fit of the GLMM modeling, and those highlighted with an asterisk (*) remained

significant ($p < 0.05$) following adjustment for multiple comparison using the FDR-based Benjamini-Hochberg method.
See also Figures S1, S3, and S7.

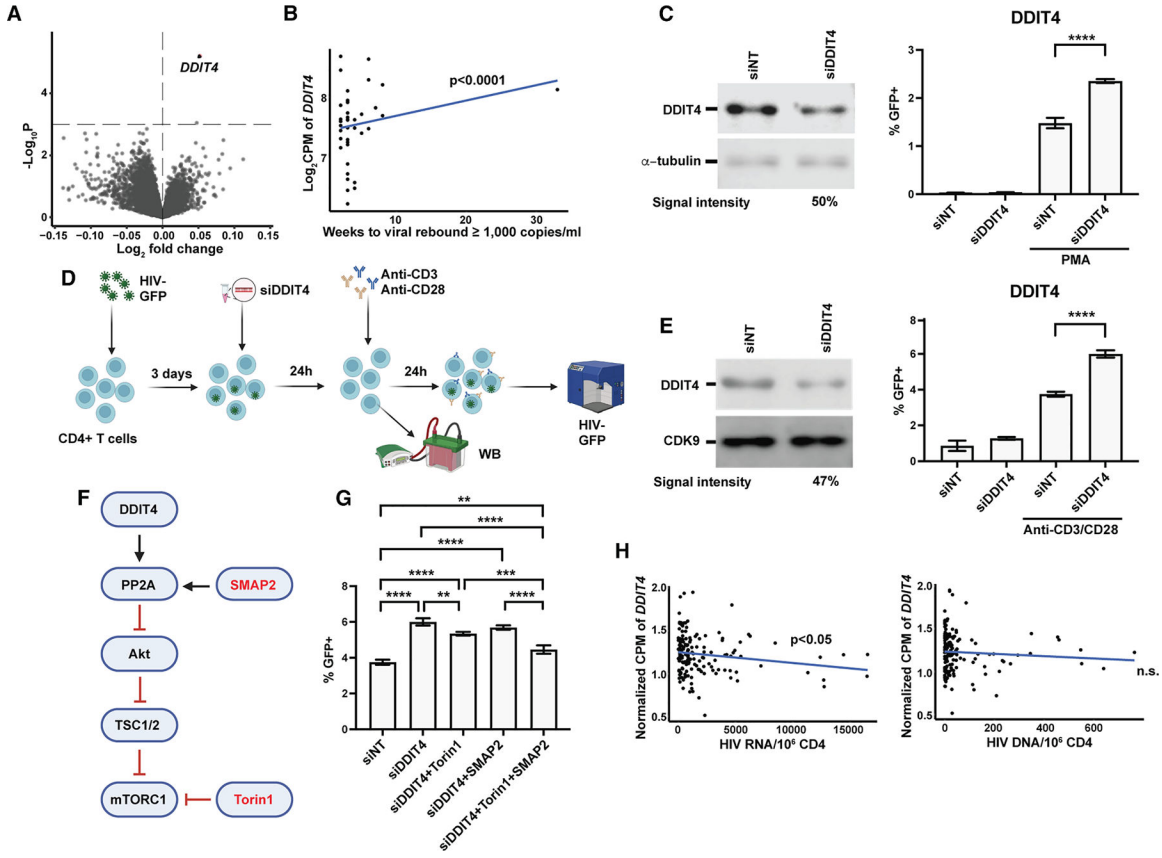

Figure 5. DDIT4 associates with increased time-to-rebound in ACTG A5345 and suppresses HIV expression

(A) Volcano plot depicting differetially expressed genes (DEGs) from RNA-seq analysis of $CD4^+$ T cells from ACTG A5345. *X* axis corresponds to slope of $\log_2$fold-change in expression per unit increase in the time-to-rebound to ≥ 1,000 HIV RNA copies/mL, with positive corresponding to genes associated with increased time-to-rebound. *Y* axis reflects the $-\log_{10}$ of the association's unadjusted *p*-value for each gene, with null hypothesis corresponding to $\log_2$fold-change = 0. Horizontal dashed line corresponds to threshold 0.001. The top DEG (*DDIT4*) as ranked by *p*-values is labeled.

(B) Association of *DDIT4* expression with time-to-rebound to ≥ 1,000 copies/mL of HIV RNA in ACTG A5345. *p*-value calculated based on fit of GLMM modeling. Counts per million, CPM.

(C) Knockdown of DDIT4 in J-Lat increases PMA-induced HIV latency reversal. Left: Western blot image showing partial knockdown of DDIT4 by siRNA as compared to non-targeting (NT) siRNA. Indicated is percentage of DDIT4 signal remaining after knockdown by siDDIT4 relative to control condition. Right: GFP, a reporter for HIV gene expression, was monitored after 2 days of treatment with NT or DDIT4 siRNA, in absence or presence of 5 nM PMA. ****$p < 0.0001$ (one-way ANOVA with multiple comparison correction by Bonferroni). Error bars depict mean with standard deviation (SD).

(D) Schematic of experimental design for DDIT4 knockdown in a primary $CD4^+$ T cell HIV latency model. Primary $CD4^+$ T cells were infected with HIV-GFP and nucleofected with siRNA. Western blot analysis was conducted to evaluate DDIT4 knockdown efficiency,

and cultures were reactivated or not with anti-CD3/CD28 with after which fluorescence-activated cell sorting (FACS) was performed.

(E) Knockdown of DDIT4 in primary model of HIV latency increases anti-CD3/CD28-induced HIV latency reversal. Left: Western blot image showing partial knockdown of DDIT4 by siRNA against DDIT4. Indicated is the percentage of DDIT4 signal remaining after knockdown by siDDIT4 relative to non-targeting siRNA (siNT). Right: GFP was monitored after 2 days of treatment with NT or DDIT4 siRNA, in absence or presence of anti-CD3/CD28 stimulation. ****$p < 0.0001$ (one-way ANOVA with multiple comparison correction by Bonferroni). Bars indicate mean with SD.

(F) Schematic of effects of DDIT4 on mTORC1 signaling. DDIT4 activates a signaling cascade which culminates in inhibition of mTOR. SMAP2 activates PP2A, while Torin1 is an mTORC1 inhibitor.

(G) DDIT4-mediated repression of HIV gene expression is mediated by inhibition of mTOR signaling. GFP expression in primary $CD4^+$ T cells was monitored after 2 days of treatment with NT or DDIT4 siRNA, in absence or presence of 10 nM of mTOR inhibitor Torin1 and/or 5 μM of the PP2A activator SMAP2. **$p < 0.01$ and ****$p < 0.0001$ (one-way ANOVA with multiple comparison correction by Bonferroni). Bars indicate mean with SD.

(H) Plots depicting *DDIT4* expression within $CD4^+$ T cells from 191 ART-suppressed PWH obtained from an RNA-seq dataset,[38] relative to HIV RNA (left) or HIV DNA (right). *p*-values were calculated based on fit of GLMM modeling. n.s. = non-significant.

See also Figures S5 and S6.

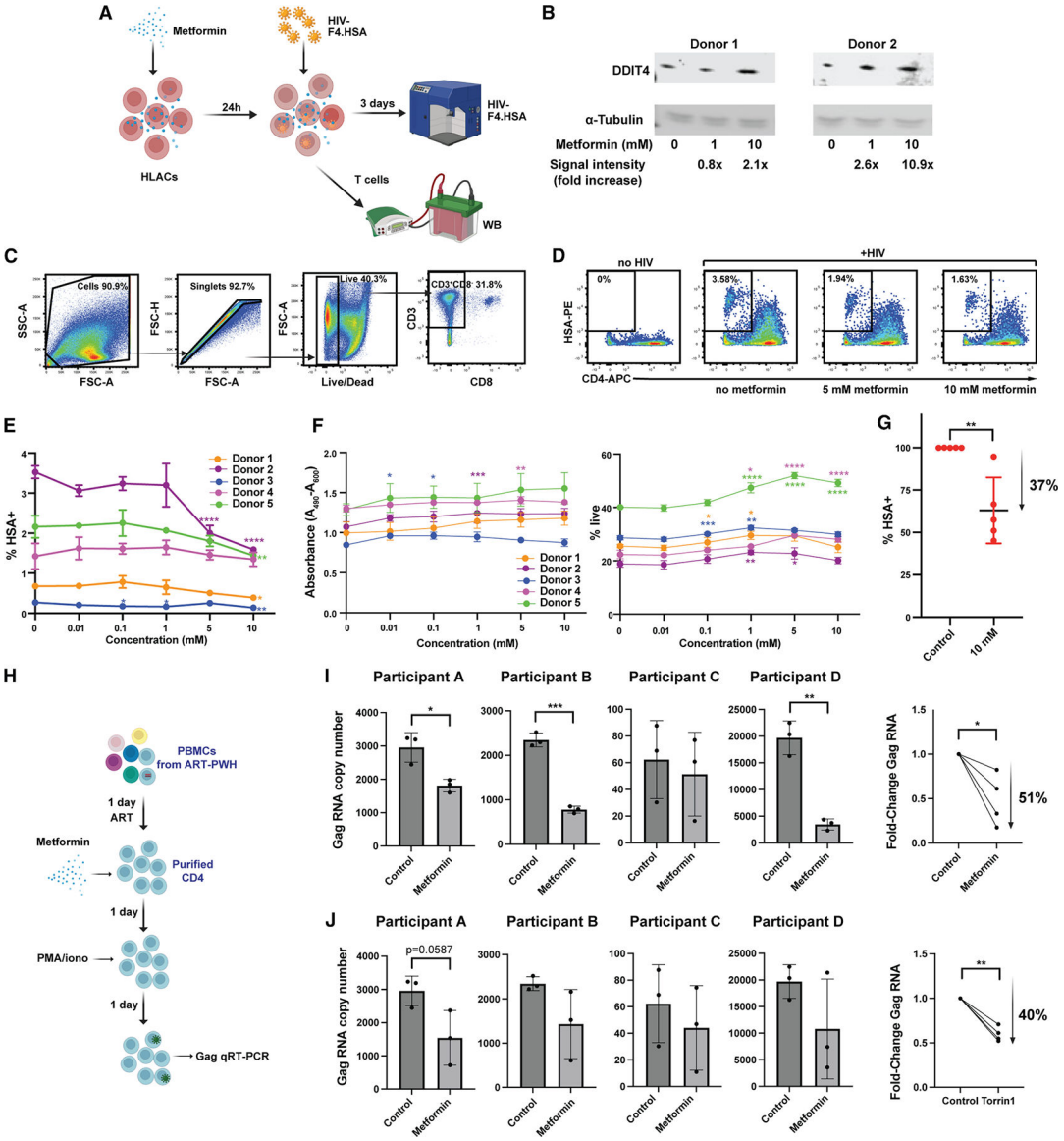

Figure 6. Metformin upregulates DDIT4 and suppresses HIV expression

(A) Schematic of experimental design to assess the impact of metformin on HIV infection of tissue-derived $CD4^+$ T cells. Human lymphoid aggregate cultures (HLACs) were treated with media alone or supplemented with metformin, after which a fraction of the culture was purified for T cells and analyzed for DDIT4 expression by western blot. Remaining HLACs were mock-treated or exposed to HIV reporter virus F4.HSA. Infection rates were monitored by FACS. (B) Western blot analysis of DDIT4 expression in purified T cells from two representative tonsil donors, with α-tubulin as loading control. Values indicate fold-increase in signal relative to 0 mM metformin.

(C) Gating strategy for FACS. Cells were gated on live singlets, followed by sub-gating on $CD3^+CD8^-$ cells.

(D and E) Representative FACS plots depicting productively infected cells ($HSA^{+}CD4^{dim}$) among $CD3^{+}CD8^{-}$ cells in absence or presence of metformin (D). Infection data from 5 independent donors are shown in (E).

(F) Cell viability as determined by lactate dehydrogenase (LDH) assay (left) or FACS viability dye (right) after treatment with indicated concentrations of metformin among infected tonsillar cultures. For (E) and (F), $*p < 0.05$, $**p < 0.01$, $***p < 0.001$, and $****p < 0.0001$, as determined by one-way ANOVA followed by Tukey's multiple comparisons test. Bars indicate mean with SD, colors represent independent donors ($n = 5$), and all conditions were performed in experimental triplicates.

(G) Metformin diminishes HIV expression by mean of 37% among infected tonsillar cultures. Plot depicts HIV infection rates in five independent donors in presence of 10 mM metformin, normalized to infection rates in absence of metformin. $**p < 0.01$ as determined by Mann-Whitney U test.

(H) Schematic of experimental design to assess impact of metformin treatment on HIV reactivation in cells from ART-suppressed PWH. Cryopreserved PBMCs from ART-suppressed PWH were cultured overnight in presence of ART, purified for $CD4^{+}$ T cells, and cultured in absence or presence of 10 mM metformin. Cells were then stimulated with PMA/ionomycin and quantitated by real-time-qPCR for HIV Gag.

(I) Metformin decreases *ex vivo* reactivation of HIV in $CD4^{+}$ T cells from ART-suppressed PWH. Cells from four participants tested in experimental triplicates are shown on the left, while line graph on the right depicts overall mean decrease (51%) in HIV Gag RNA among the donors.

(J) Torin1 decreases reactivation of HIV in cells from ART-suppressed PWH. Experiment was performed as detailed in (H) but using Torin1 instead of metformin, and data depicted as in (I). HIV RNA induction was decreased by a mean of 40% among the donors. $*p < 0.05$, $**p < 0.01$, and $***p < 0.001$ (unpaired Student's *t* test).

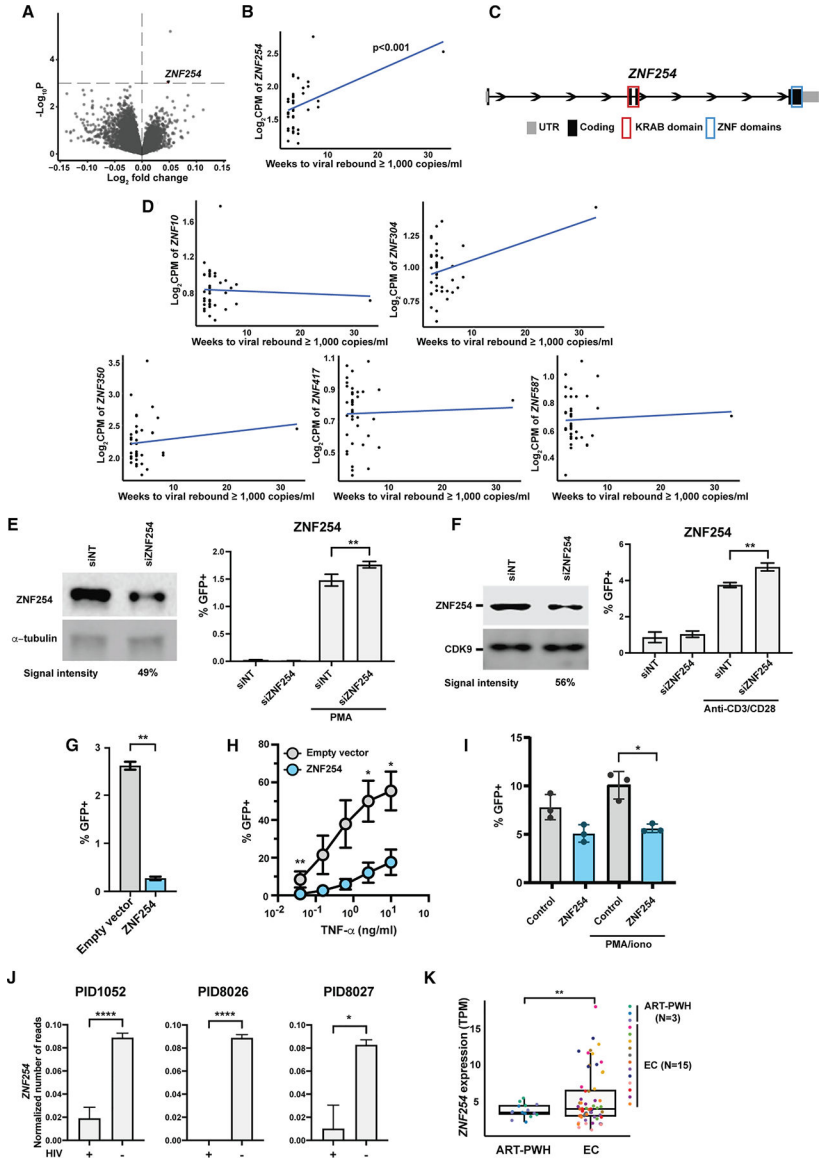

Figure 7. ZNF254 associates with increased time-to-rebound in ACTG A5345 and suppresses HIV expression

(A) Volcano plot depicting DEGs from RNA-seq analysis of CD4$^+$ T cells from ACTG A5345, highlighting *ZNF254*.

(B) Association of *ZNF254* expression with time-to-rebound to ≥ 1,000 copies/mL of HIV RNA in ACTG A5345. *p*-value calculated based on fit of GLMM modeling.

(C) Genomic structure *ZNF254* gene. Untranslated regions (UTRs) are depicted as gray boxes, while coding regions are depicted as black boxes. Regions encoding the KRAB and ZNF domains are outlined in red and blue, respectively. Arrows along genes indicate transcriptional direction.

(D) Associations of *ZNF10*, *ZNF304*, *ZNF350*, *ZNF417*, and *ZNF587* with time-to-rebound to ≥ 1,000 copies/mL of HIV RNA in ACTG A5345. For (B) and (D), *p*-values were calculated based on fit of GLMM modeling.

(E) Knockdown of ZNF254 in J-Lat cell line increases PMA-induced HIV latency reversal. Left: Western blot image showing partial knockdown of ZNF254 by siRNA against ZNF254. Indicated is percentage of ZNF254 signal remaining after knockdown by siZNF254 relative to control condition. Right: GFP was monitored after 2 days of treatment with NT or ZNF254 siRNA, in absence or presence of 5 nM PMA. $^{**}p < 0.01$ (one-way ANOVA with multiple comparison correction by Bonferroni). Bars indicate mean with SD.

(F) Knockdown of ZNF254 in primary model of HIV latency increases anti-CD3/CD28-induced HIV latency reversal. Left: Western blot image showing partial knockdown of ZNF254 by siRNA against ZNF254. Indicated is the percentage of ZNF254 signal remaining after knockdown by siZNF254 relative to siNT. Right: GFP was monitored after treatment with NT or ZNF254 siRNA, in absence or presence of anti-CD3/CD28 stimulation. $^{**}p < 0.01$ (one-way ANOVA with multiple comparison correction by Bonferroni). Bars indicate mean with SD.

(G) ZNF254 overexpression suppresses basal HIV gene expression in J-Lat. J-Lat cells were transduced with ZNF254 or empty vector and monitored for GFP. $^{**}p < 0.01$ (unpaired Student's *t* test).

(H) ZNF254 overexpression suppresses TNFα-induced HIV gene expression in J-Lat. J-Lat cells were transduced as in (G) and treated with indicated concentrations of TNFα. $^{*}p < 0.05$ and $^{**}p < 0.01$ (Welch's *t* test with Holm-Sidak correction).

(I) ZNF254 overexpression suppresses HIV expression in primary $CD4^+$ T cells. HIV-infected primary $CD4^+$ T cells were transduced with ZNF254 or control vector, stimulated or not with PMA/ionomycin, and monitored for GFP. $^{*}p < 0.05$ (paired Student's *t* test).

(J) Assessment of *ZNF254* expression among HIV RNA^+ (vs. HIV RNA^-) $CD4^+$ T cells identified by HIV-seq from three ART-suppressed PWH (PID1052, PID8026, and PID8027).[50] $^{*}p < 0.05$ and $^{****}p < 0.0001$ as determined by Welch's *t* test.

(K) Box plots of distribution of normalized *ZNF254* expression across 75 sorted $CD4^+$ T cell subsets from ART-suppressed PWH ($n = 15$, corresponding to five subsets from each of 3 donors) and ECs ($n = 60$, corresponding to 5 subsets from each of 12 donors). Boxes represent IQR, with horizontal line indicating median expression. $^{**}p < 0.01$ by Welch's *t* test for unequal variances. TPM, transcripts per million.

See also Figures S5 and S6.

KEY RESOURCES TABLE

REAGENT or RESOURCE	SOURCE	IDENTIFIER
Antibodies		
CD49d 141Pr (9F10)	Standard BioTools	Cat# 3141004B; RRID: AB_2892684
CD19 142Nd (HIB19)	Standard BioTools	Cat# 3142001B; RRID: AB_2651155
CCR5 144Nd (NP6G4)	Standard BioTools	Cat# 3144007A; RRID: AB_2661814
CD8 146Nd (RPA-T8)	Standard BioTools	Cat# 3146001B; RRID: AB_2687641
CD7 147Sm (CD76B7)	Standard BioTools	Cat# 3147006B; RRID: AB_2802104
ICOS 148Nd (C398.4A)	Standard BioTools	Cat# 3148019B; RRID: AB_2756435
CD73 150Nd (AD2)	BioLegend	Cat# 344002; RRID: AB_1877158
CD103 151Eu (Ber-ACT8)	Standard BioTools	Cat# 3151011B; RRID: AB_2756418
CD62L 153Eu (DREG56)	Standard BioTools	Cat# 3153004B; RRID: AB_2810245
TIGIT 154Sm (MBSA43)	Standard BioTools	Cat# 3154016B; RRID: AB_2756419
CCR6 155Gd (11A9)	BD Biosciences	Cat# 559560; RRID: AB_10916526
CD29 156Gd (TS2/16)	Standard BioTools	Cat# 3156007B; RRID: AB_3086682
OX40 158Gd (ACT35)	Standard BioTools	Cat# 3158012B; RRID: AB_2905646
CCR7 159Tb (G043H7)	Standard BioTools	Cat# 3159003A; RRID: AB_2661804
CD28 160Gd (CD28.2)	Standard BioTools	Cat# 3160003B; RRID: AB_2868400
CD45RO 161Dy (UCHL1)	BioLegend	Cat# 304239; RRID: AB_314418
CD69 162Dy (FN50)	Standard BioTools	Cat# 3162001B; RRID: AB_2687849
CRTH2 163Dy (BM16)	Standard BioTools	Cat# 3163003B; RRID: AB_2810253
PD-1 164Dy (EH12.1)	BD Biosciences	Cat# 562138; RRID: AB_10892876
CD127 165Ho (A019D5)	Standard BioTools	Cat# 3165008B; RRID: AB_2868401
CXCR5 166Er (RF8B2)	BD Biosciences	Cat# 552032; RRID: AB_394324
CD27 167Er (L128)	Standard BioTools	Cat# 3167006B; RRID: AB_2687645
CD30 168Er (BerH8)	BD Biosciences	Cat# 555827; RRID: AB_393541
CD45RA 169Tm (HI100)	Standard BioTools	Cat# 3169008B; RRID: AB_2651156
CD3 170Er (UCHT1)	Standard BioTools	Cat# 3170001B; RRID: AB_2661807
CD57 171Yb (HCD57)	BioLegend	Cat# 359602; RRID: AB_2562403
CD38 172Yb (HIT2)	Standard BioTools	Cat# 3172007B; RRID: AB_2756288
α4β7 173Yb (Act1)	In-house	In-house; no RRID
CD4 174Yb (SK3)	Standard BioTools	Cat# 3174004B; RRID: AB_2687862

REAGENT or RESOURCE	SOURCE	IDENTIFIER
CXCR4 175Lu (12G5)	Standard BioTools	Cat# 3175001B; RRID: AB_3678029
CD25 176Yb (M-A251)	BD Biosciences	Cat# 555430; RRID: AB_395824
HLA-DR 112Cd (Tu36)	ThermoFisher	Cat# Q22158; RRID: AB_10401403
RORγt 115Di (AFKJS-9)	ThermoFisher	Cat# 14-6988-82; RRID: AB_1834475
NFAT1 143Nd (D43B1)	Standard BioTools	Cat# 3143023A; RRID: AB_2810851
Survivin 145Nd (91630)	R&D Systems	Cat# MAB886; RRID: AB_2243438
T-bet 149Sm (eBio4B10)	ThermoFisher	Cat# 14-5825-82; RRID: AB_925761
Blimp-1 152Sm (6D3)	BD Biosciences	Cat# 564703; RRID: AB_1907437
CTLA-4 157Gd (14D3)	ThermoFisher	Cat# 14-1529-82; RRID: AB_467512
CD3 (APC/Cy7) (clone SK7)	BioLegend	Cat# 344818; RRID: AB_10645474
CD8 (Alexa Fluor 700) (clone SK1)	BioLegend	Cat# 344724; RRID: AB_2562790
CD24/HSA (PE) (clone M1/69)	BD Biosciences	Cat# 553262; RRID: AB_394741
CD25 141Pr (M-A251)	BD Biosciences	Cat# 555430; RRID: AB_395824
CD14 142Nd (M5E2)	Biolegend	Cat# 301843; RRID: AB_2562813
CD33 142Nd (WM53)	Biolegend	Cat# 303402; RRID: AB_314346
LILRB1 143Nd (GHI/75)	Biolegend	Cat# 333702; RRID: AB_2756420
Siglec-7 145Nd (S7.7)	Biolegend	Cat# 347702; RRID: AB_2189411
NKp30 150Nd (P30-15)	Biolegend	Cat# 325202; RRID: AB_756106
NKp46 151Eu (9E2)	Biolegend	Cat# 331902; RRID: AB_1027637
TCRgd 152Sm (11F2)	Standard Biotools	Cat# 3152008B; RRID: AB_2687643
NKG2D 156Gd (1D11)	Biolegend	Cat# 320802; RRID: AB_492956
KIR2DL1 157Gd (143211)	R&D Systems	Cat# MAB1844-100; RRID: AB_2130400
2B4 168Er (C1.7)	Biolegend	Cat# 329502; RRID: AB_1279194
NKG2A 171Yb (131411)	R&D Systems	Cat# 131411; RRID: AB_3657313
KIR3DL1 173Yb (DX-9)	BD Biosciences	Cat# 555964; RRID: AB_396258
CD56 176Yb (NCAM16.2)	Standard Biotools	Cat# 3176008B; RRID: AB_2938870
CD57 89Y (HNK-1)	Biolegend	Cat# 359602; RRID: AB_2562403
CD33 115In (WM53)	Biolegend	Cat# 303402; RRID: AB_314346
CD94 143Nd (DX22)	Biolegend	Cat# 305502; RRID: AB_314532
CD2 144Nd (TS1/8)	Biolegend	Cat# 309219; RRID: AB_2563727
2B4 145Nd (C1.7)	Biolegend	Cat# 329502; RRID: AB_1279194

REAGENT or RESOURCE	SOURCE	IDENTIFIER
TIM-3 148Nd (F38-2E2)	Biolegend	Cat# 345019; RRID: AB_2563790
NKG2D 149Sm (1D11)	Biolegend	Cat# 320802; RRID: AB_492956
LAG-3 150Nd (11C3C65)	Standard Biotools	Cat# 3150030B; RRID: AB_3661851
CD107a 151Eu (H4A3)	Standard Biotools	Cat# 3151002B; RRID: AB_3677850
NKp46 152Sm (9E2)	Biolegend	Cat# 331902; RRID: AB_1027637
NKG2C 155Gd (S19005E)	Biolegend	Cat# 375002; RRID: AB_2888870
LILRB1 156Gd (GHI/75)	Standard Biotools	Cat# 3156020B; RRID: AB_2756420
NTB-A 157Gd (NT-7)	Biolegend	Cat# 317202; RRID: AB_571931
KIR2DL1 158Gd (HP-DM1)	Biolegend	Cat# 374904; RRID: AB_2832735
NKp30 159Tb (Z25)	Standard Biotools	Cat# 3159017B; RRID: AB_3677903
CXCR6 160Gd (K041E5)	Standard Biotools	Cat# 3160016B; RRID: AB_3677914
Ki67 161Dy (B56)	Standard Biotools	Cat# 3161007B; RRID: AB_2811255
CD49a 163Dy (TS2/7)	Standard Biotools	Cat# 3163015B; RRID: AB_2893061
CD19 165Ho (HIB19)	Standard Biotools	Cat# 3165025B; RRID: AB_3677967
Siglec-7 166Er (6-434)	Standard Biotools	Cat# 3166019B; RRID: AB_3677976
KIR3DL1 167Er (DX9)	Standard Biotools	Cat# 3167013B; RRID: AB_3677982
DNAM-1 168Er (11A8)	Biolegend	Cat# 338302; RRID: AB_1279155
NKG2A 169Tm (Z199)	Standard Biotools	Cat# 3169013B; RRID: AB_2756426
CXCR5 171Yb (RF8B2)	Standard Biotools	Cat# 3171014B; RRID: AB_2858239
KIR2DL2/L3 173Yb (DX27)	Standard Biotools	Cat# 3173010B; RRID: AB_3678016
TCF1 175Lu (7F11A10)	Biolegend	Cat# 655202; RRID: AB_2562103
CD16 209Bi (3G8)	Standard Biotools	Cat# 3209002B; RRID: AB_2756431
α-tubulin	Sigma	Cat# CP06
CDK9	Bethyl	Cat# A303-493A
DDIT4	Bethyl	Cat# A302-169A
α-ZNF254	Novusbio	Cat# H00009534-B01P
goat anti-mouse-680 nm	Thermo Fisher	Cat# A-21057
goat anti-rabbit-680 nm	Thermo Fisher	Cat# A-21076
CD28	BD Biosciences	Cat# 555725
CD3	BD Biosciences	Cat# 555336
Bacterial and virus strains		

REAGENT or RESOURCE	SOURCE	IDENTIFIER
HIV-F4.HSA (NL-HSA.6ATRi-C.109FPB4.ecto)	PMID 28746881	N/A
Biological samples		
PBMCs from people with HIV	ACTG A5345, REDUC, TEACH, CLEAR,	N/A
Tonsils from people without HIV	Cooperative Human Tissue Network (CHTN)	N/A
PBMCs from people without HIV	https://www.vitalant.org	N/A
Chemicals, peptides, and recombinant proteins		
Human TruStain FcX™ Fc Block	BioLegend	Cat# 422302; RRID: AB_2818986
Fetal Bovine Serum	VWR	Cat# 97068-085
RPMI-1640 medium	Corning	Cat# 10-040-CM
Lymphoprep density gradient medium	StemCell Technologies	Cat# 07851
Penicillin-Streptomycin-Glutamine	Thermo Fisher Scientific	Cat# 10378016
Metal Contaminant-Free PBS	Rockland	Cat# MB-008
Normal Mouse Serum	Thermo Fisher Scientific	Cat# 10410
Normal Rat Serum	Thermo Fisher Scientific	Cat# 10710C
Human Serum from Male AB Plasma	Sigma-Aldrich	Cat# H4522
Iridium Interchelator Solution	Standard Biotools	Cat# 201192B
EQ Four Element Calibration Beads	Standard Biotools	Cat# 201078
BD CompBeads	BD Biosciences	Cat# 555843
16% Paraformaldehyde	Electron Microscopy Sciences	Cat# 15710
Antibiotic-Antimycotic Solution, 100X	Corning	Cat# 30-004-CI
DNase I	Sigma	Cat# 11284932001
Phorbol 12-myristate 13-acetate (PMA)	Selleckchemor	Cat# S7791
Torin	Selleckchem	Cat# S2827
SMAP-2	MedChemExpress HY	Cat# 120272
Metformin	Sigma-Aldrich	Cat# PHR1084
Puromycin	Thermo Fisher	Cat# A1113803
Doxycycline	StemCell Technologies	Cat# 72742
Critical commercial assays		
MaxPar X8 Antibody Labeling Kit	Standard Biotools	Cat# 201169B
Cell-ID 20-Plex Pd Barcoding Kit	Standard Biotools	Cat# 205060
Foxp3 Transcription Factor Staining Buffer Set	eBioscience	Cat# 00-5523-00

REAGENT or RESOURCE	SOURCE	IDENTIFIER
MaxPar Cell Acquisition Solution	Standard Biotools	Cat# 201240
MaxPar PBS	Standard Biotools	Cat# 201058
MaxPar Cell Staining Buffer	Standard Biotools	Cat# 201068
LentiX p24Gag Rapid Titer Kit	Takara Bio Inc	Cat# 632200
Zombie Aqua™ Fixable Viability Kit	BioLegend	Cat# 423102;
NULISAseq Inflammation Panel 250	Alamar Biosciences	https://alamarbio.com/products-and-services/nulisa-inflammation-panel/
EasySep™ Human CD4+ T Cell Isolation Kit	StemCell Technologies	Cat# 100-0696
NEB Next Ultra II RNA Library Prep Kit for Illumina	New England Biolabs	Cat# E7770
Deposited data		
Raw CyTOF datasets	This paper	http://datadryad.org/share/GGND55gKi_JGqv-48c2uKc3yxMwKI7rioHbwm9FKRzY
Raw RNAseq data	This paper	Gene Expression Omnibus (GEO) database under accession number GSE290636
Recombinant DNA		
pHIV-F4-HSA (pNL-HSA.6ATRi-C109FPB4.ecto)	Cavrois et al. (PMID 28746881)	N/A
Software and algorithms		
FlowJo software (Version 10.10.0)	https://www.flowjo.com/	RRID: SCR_008520
GraphPad Prism (Version 10.2.0)	http://www.graphpad.com/	RRID: SCR_002798
RStudio (2024.12.0 + 467 “Kousa Dogwood” Release)	https://rstudio.com/	RRID: SCR_000432
R Project for Statistical Computing (Version 4.5.0)	http://www.r-project.org/	RRID: SCR_001905
ggplot2	https://cran.r-project.org/web/packages/ggplot2/index.html	RRID: SCR_014601
edgeR	https://bioconductor.org/packages/release/bioc/html/edgeR.html	RRID: SCR_012802
Seurat	https://satijalab.org/seurat/get_started.html	RRID: SCR_016341
EnhancedVolcano	https://bioconductor.org/packages/release/bioc/html/EnhancedVolcano.html	RRID: SCR_018931
Harmony	https://github.com/immunogenomics/harmony	RRID: SCR_022206

REAGENT or RESOURCE	SOURCE	IDENTIFIER
RandomForest	https://cran.r-project.org/web/packages/randomForest/	RRID: SCR_015718
clusterProfiler	https://www.bioconductor.org/packages/release/bioc/html/clusterProfiler.html	RRID: SCR_016884
lme4	https://cran.r-project.org/web/packages/lme4/index.html	RRID: SCR_015654
emmeans	https://CRAN.R-project.org/package=emmeans	RRID: SCR_018734